https://doi.org/10.5194/acp-2020-442
Preprint. Discussion started: 25 May 2020
© Author(s) 2020. CC BY 4.0 License.

Atmospheric Chemistry and Physics Discussions

# On mineral dust aerosol hygroscopicity

Lanxiadi Chen,[1,6] Chao Peng,[1] Athanasios Nenes,[2,5] Wenjun Gu,[1,6] Hanjing Fu,[3] Xing Jian,[3] Huanhuan Zhang,[1,6] Guohua Zhang,[1] Jianxi Zhu,[4] Xinming Wang,[1,6,7] Mingjin Tang[1,6,7,*]

[1] State Key Laboratory of Organic Geochemistry, Guangdong Key Laboratory of Environmental Protection and Resources Utilization, and Guangdong-Hong Kong-Macao Joint Laboratory for Environmental Pollution and Control, Guangzhou Institute of Geochemistry, Chinese Academy of Sciences, Guangzhou 510640, China

[2] Civil and Environmental Engineering, École Polytechnique Fédérale de Lausanne (EPFL), Lausanne, Switzerland

[3] State Key Laboratory of Marine Environmental Science, College of Ocean and Earth Sciences, Xiamen University, Xiamen, China

[4] CAS Key Laboratory of Mineralogy and Metallogeny and Guangdong Provincial Key Laboratory of Mineral Physics and Material Research and Development, Guangzhou Institute of Geochemistry, Chinese Academy of Sciences, Guangzhou, China

[5] Institute of Chemical Engineering Sciences, Foundation for Research and Technology-Hellas, Patras, Greece

[6] University of Chinese Academy of Sciences, Beijing, China

[7] Center for Excellence in Regional Atmospheric Environment, Institute of Urban Environment, Chinese Academy of Sciences, Xiamen, China

* Correspondence: Mingjin Tang (mingjintang@gig.ac.cn)

https://doi.org/10.5194/acp-2020-442
Preprint. Discussion started: 25 May 2020
© Author(s) 2020. CC BY 4.0 License.

Atmospheric Chemistry and Physics Discussions


## Abstract

Despite its importance, hygroscopicity of mineral dust aerosol remains highly uncertain. In this work, we investigated water adsorption and hygroscopicity of different mineral dust samples at 25 °C, via measuring sample mass at different relative humidity (RH, up to 90%) using a very sensitive balance. Mineral dust samples examined (twenty one in total) included seven authentic mineral dust samples from different regions in the world and fourteen major minerals contained in mineral dust aerosol. At 90% RH, mass ratios of adsorbed water to the dry mineral ranged from 0.0011 to 0.3080, largely depending on the BET surface areas of mineral dust samples. The surface coverages of adsorbed water were determined to vary between 1.26 and 8.63 at 90% RH, and it was found that the Frenkel-Halsey-Hill (FHH) adsorption isotherm could well describe surface coverages of adsorbed water as a function of RH, with $A_{FHH}$ and $B_{FHH}$ parameters in the range of 0.15-4.39 and 1.10-1.91, respectively. The comprehensive and robust data obtained would largely improve our knowledge of hygroscopicity of mineral dust aerosol.

https://doi.org/10.5194/acp-2020-442
Preprint. Discussion started: 25 May 2020
© Author(s) 2020. CC BY 4.0 License.

Atmospheric Chemistry and Physics Discussions

## 1 Introduction

Mineral dust aerosol mainly comes from arid and semi-arid areas (Ginoux et al., 2012), such as Saharan desert, Taklimakan desert, and etc. Its annual flux and atmospheric loadings are estimated to be ~2000 Tg $yr^{-1}$ and ~19 Tg (Textor et al., 2006; Huneeus et al., 2011), making mineral dust one of the most important aerosols in the troposphere. Mineral dust aerosol has significant impacts on atmospheric chemistry, climate and biogeochemical cycles (Knippertz and Stuut, 2014). It can alter the radiative forcing of the earth both directly (Balkanski et al., 2007; Huang et al., 2014; Di Biagio et al., 2017) and indirectly (Cziczo et al., 2013; Karydis et al., 2017). Mineral dust can also change the abundance of reactive trace gases as well as aerosol compositions via heterogeneous reactions (Usher et al., 2003; Dupart et al., 2012; He et al., 2014; Tang et al., 2017; Yu and Jang, 2019). Furthermore, the deposition of mineral dust will bring substantial amounts of nutrients (e.g., Fe and P) into some marine and terrestrial ecosystems, thereby largely affecting biogeochemistry in these regions (Jickells et al., 2005; Okin et al., 2011; Schulz et al., 2012; Li et al., 2017; Tagliabue et al., 2017; Meskhidze et al., 2019).

Hygroscopicity largely determines the impacts of mineral dust aerosol on atmospheric chemistry and climate. For examples, many studies found that relative humidity (RH) and thus the amount of water associated with mineral dust have profound effects on the rates, mechanisms and products of heterogeneous reactions (Vlasenko et al., 2009; Rubasinghege and Grassian, 2013; Tang et al., 2014; Tang et al., 2017; Lasne et al., 2018; Wang et al., 2018; Yu and Jang, 2018; Mitroo et al., 2019). In addition, hygroscopicity of mineral dust aerosol plays important roles in its optical properties (and thus the direct radiative effect) and its ability to act as cloud condensation nuclei and ice-nucleating particles (and thus the indirect radiative effect) (Sorjamaa and Laaksonen, 2007; Kumar et al., 2009; Garimella et al., 2014; Kreidenweis and Asa-Awuku, 2014; Laaksonen

https://doi.org/10.5194/acp-2020-442
Preprint. Discussion started: 25 May 2020
© Author(s) 2020. CC BY 4.0 License.

Atmospheric Chemistry and Physics Discussions

et al., 2016; Tang et al., 2016; Tang et al., 2019a). Therefore, a number of previous studies have investigated water adsorption and hygroscopic properties of mineral dust aerosol at <100% RH, as reviewed by Tang et al. (2016). However, different studies displayed considerable discrepancies as large as a few orders of magnitude (Tang et al., 2016), thus precluding a good understanding of the roles mineral dust aerosol plays in atmospheric chemistry and climate.

As pointed out by Tang et al. (2016), such discrepancies are largely due to the non-sphericity and low hygroscopicity of mineral dust particles, making it difficult to quantify the amount of water associated with them at elevated RH. Instruments which measure mobility or optical diameters of aerosol particles often found that the diameters of mineral dust particles did not increase significantly (or even showed considerable decrease due to particle restructuring during humidification) with increasing RH (Gustafsson et al., 2005; Vlasenko et al., 2005; Herich et al., 2009; Koehler et al., 2009; Attwood and Greenslade, 2011). Fourier transform infrared spectroscopy (FTIR) is a sensitive method to detect adsorbed water on mineral dust (Goodman et al., 2001; Ma et al., 2010a; Joshi et al., 2017); however, it is not a trivial task to convert the intensity of its infrared absorption to the amount of adsorbed water (Schuttlefield et al., 2007b; Ma et al., 2010b; Tang et al., 2016). Quartz crystal microbalance (QCM) is another sensitive technique to examine water adsorption and absorption (Schuttlefield et al., 2007b; Navea et al., 2010; Yeşilbaş and Boily, 2016); however, it is in doubt that the underlying assumptions required to convert the change in resonance frequency of the quartz crystal to the change in sample mass are always fulfilled (Tang et al., 2016; Tang et al., 2019a).

In our previous work (Gu et al., 2017), we developed a new method to investigate hygroscopic properties of atmospherically relevant particles using a vapor sorption analyzer, in which a very sensitive balance was employed to measure the mass of a sample (typically with a

https://doi.org/10.5194/acp-2020-442
Preprint. Discussion started: 25 May 2020
© Author(s) 2020. CC BY 4.0 License.

Atmospheric Chemistry and Physics Discussions

dry mass of tenths or a few mg) as different RH under isotherm conditions. Comprehensive validation carried out confirmed the robustness of this method (Gu et al., 2017), and this instrument has been employed to study hygroscopic properties of various particles, including nonspherical particles such as saline mineral dust and pollen grains (Chen et al., 2019; Tang et al., 2019b; Tang et al., 2019c). This instrument was used in the present work to quantitatively measure hygroscopic properties of a number of mineral dust particles, including several authentic mineral dust samples from different regions in the world and individual minerals commonly found in mineral dust aerosol. We also attempted to figure out which theoretical models could describe hygroscopic properties of mineral dust particles, and examined the dependence of mineral dust hygroscopicity on several parameters (such as particle diameter, surface area and the mass fraction of soluble materials).

# 2 Experimental section

## 2.1 Sample information

In total twenty one different types of mineral dust were investigated, including fourteen major minerals commonly found in mineral dust aerosol (Formenti et al., 2011; Nickovic et al., 2012; Journet et al., 2014; Scanza et al., 2015; Engelbrecht et al., 2016) and seven authentic mineral dust samples, and their information can be found in Table 1. The fourteen major minerals examined included four oxides ($SiO_2$, $TiO_2$, magnetite and hematite), one oxyhydroxide (goethite), three feldspars (potassium feldspar, albite and microcline), two carbonates ($CaCO_3$ and dolomite) and four clay minerals (montmorillonite, illite, kaolinite and chlorite). As shown in Table 1, $SiO_2$, montmorillonite and kaolinite were supplied by Sigma Aldrich; $TiO_2$ (P25) was supplied by Degussa; hematite and magnetite were supplied by Strem; goethite was provided by Santa Cruz; microcline, $CaCO_3$ and dolomite were provided by Alfa Aesar. Potassium feldspar and albite were

https://doi.org/10.5194/acp-2020-442
Preprint. Discussion started: 25 May 2020
© Author(s) 2020. CC BY 4.0 License.

Atmospheric Chemistry and Physics Discussions

obtained from National Research Center of Testing Techniques for Building Materials (NRCTTBM, Beijing, China), and illite (IMt-1) was obtained from the Clay Mineral Society at Purdue University, Indianan, USA (Schuttlefield et al., 2007b; Tang et al., 2014). In addition, chlorite was collected by one co-author from Liaoning Province, China.

**Table 1.** Measured BET surface areas (BET), average particle diameters ($d_p$) and sources of mineral dust samples examined in this work.

| sample | BET ($m^2/g$) | $d_p$ (μm) | source |
|---|---|---|---|
| $SiO_2$ | 6.54±0.01 | 1.65 | Sigma Aldrich |
| $TiO_2$ | 54.60±0.01 | 1.66 | Degussa |
| hematite | 9.23±0.17 | 0.80 | Strem |
| goethite | 13.41±0.01 | 1.00 | Santa Cruz |
| magnetite | 6.34±0.04 | 1.70 | Strem |
| potassium feldspar | 3.96±0.01 | 8.25 | NRCTTBM |
| albite | 3.62±0.02 | 5.51 | NRCTTBM |
| microcline | 2.17±0.01 | 14.33 | Alfa Aesar |
| $CaCO_3$ | 2.18±0.01 | 3.12 | Alfa Aesar |
| dolomite | 11.79±0.05 | 7.41 | Alfa Aesar |
| illite | 24.04±0.14 | 20.23 | The Clay Minerals Society |
| kaolinite | 9.64±0.01 | 9.99 | Sigma Aldrich |
| montmorillonite | 249.91±0.42 | 23.95 | Sigma Aldrich |
| chlorite | 9.95±0.03 | 19.19 | Liaoning, China |
| ATD | 36.67±1.06 | 1.05 | Powder Technology Inc. |
| China loess | 11.71±0.02 | 2.44 | Chinese Academy of Geological Science |
| QH dust | 8.79±0.02 | 18.56 | Chinese Academy of Geological Science |
| TLF dust | 8.49±0.01 | 8.04 | Turpan, Xinjiang, China |
| Bordj dust | 16.40±1.20 | 32.30 | M'Bour, Algeria |
| M'Bour dust | 14.50±1.00 | 54.41 | Bordj, Senegal |
| Saharan dust | 51.46±0.34 | 23.70 | Cape Verde |

https://doi.org/10.5194/acp-2020-442
Preprint. Discussion started: 25 May 2020
© Author(s) 2020. CC BY 4.0 License.

Atmospheric Chemistry and Physics Discussions

116 The seven authentic mineral dust samples were obtained from Africa, Asia and North
117 America. As shown in Figure 1, three authentic mineral dust samples (M'Bour dust, Bordj dust
118 and Saharan dust) were collected from topsoil in Senegal, Algeria and Cape Verde Islands (Tang
119 et al., 2012; Joshi et al., 2017), respectively. QH dust (which is brown desert soil) and China loess,
120 collected from topsoil in Qinghai and Shaanxi, were supplied by Chinese Academy of Geological
121 Science as certificated materials (GBW07448 and GBW07454) (Tang et al., 2019c). TLF dust
122 were airborne dust particles collected on 23 April 2010 at an urban site in Turpan (Xinjiang, China)
123 during a major dust storm. In addition, Arizona Test Dust (ATD, nominal 0-3 μm fraction), an
124 authentic mineral dust sample commercially available from Powder Technology Inc. (Minnesota,
125 USA) and widely used in atmospheric aerosol research (Vlasenko et al., 2005; Sullivan et al.,
126 2010a; Tang et al., 2016), was also investigated in our work.

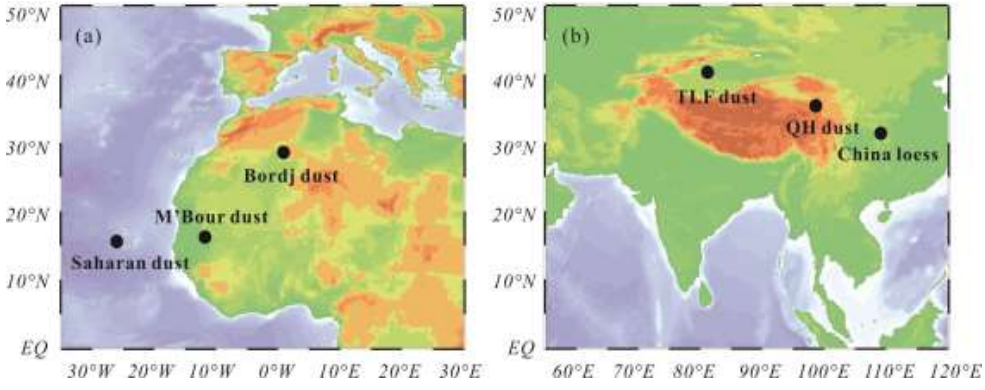


127

128 **Figure 1.** Locations where (a) African and (b) Asian authentic mineral dust samples examined in
129 this work were collected.

130

131 When received, three feldspars, dolomite, illite, chlorite and TLF dust contained significant
132 amounts of rock chips or giant particles; as a result, they were pretreated using the procedure
133 described in our previous work (Tang et al., 2019c). In brief, these samples were dried at 120 °C

https://doi.org/10.5194/acp-2020-442
Preprint. Discussion started: 25 May 2020
© Author(s) 2020. CC BY 4.0 License.

Atmospheric Chemistry and Physics Discussions

for 24 hours using an oven; after that, they were ground manually and then using a ball mill so that most particles were <74 μm in diameter; finally, these samples were dried again at 120 $^{o}$C for 24 hours and then cooled down. All the samples were stored in plastic bottles which were tightly sealed to prevent contamination by lab air.

**2.2 Sample characterization**

Dynamic light scattering (JL-1177, Jingxin Powder Technologies Inc., Chengdu, Sichuan, China) was employed to measure size distributions of mineral dust samples examined in our work. In addition, Brunauer-Emmett-Teller (BET) surface areas of these samples were determined using an accelerated surface area and porosimetry analyzer (ASAP 2020 PLUS, Micromeritics, Georgia, USA), and $N_2$ was used as the adsorbate. Details on particle size and BET surface area measurements can be found elsewhere (Li et al., 2020).

To measure their inorganic soluble compositions, each mineral dust sample (~10 mg) was mixed with 10 mL ultrapure deionized water, and the mixture was stirred for 2 hours using an oscillating table. After centrifugalization, the solution was filtered using a 5 mL syringe fitted with a 0.2 μm PTFE membrane filter and then analyzed using ion chromatography (Metrohm model 761 Compact IC, Metrohm, Herisau, Switzerland). More information on ion chromatography analysis can be found in our previous work (Tang et al., 2019c). We attempted to measure five cations ($Na^+$, $K^+$, $NH_4^+$, $Mg^{2+}$ and $Ca^{2+}$) and seven anions ($NO_3^-$, $SO_4^{2-}$, $Cl^-$, $NO_2$-, $Br^-$, $F^-$ and $PO_4^{3-}$), and their detection limits were estimated to be around 0.02 mg/L.

**2.3 Hygroscopicity measurements**

Hygroscopic properties of mineral dust samples were investigated using a vapor sorption analyzer (Q5000SA, TA instruments, Delaware, USA). This instrument, described in our previous work (Gu et al., 2017; Chen et al., 2019; Tang et al., 2019b), measured sample mass as a function

https://doi.org/10.5194/acp-2020-442
Preprint. Discussion started: 25 May 2020
© Author(s) 2020. CC BY 4.0 License.

Atmospheric Chemistry and Physics Discussions

of RH under isotherm conditions. Measurements could be conducted in the RH range of 0-98% and in the temperature range of 5-85 °C. We routinely measured the deliquescence RH of NaCl, $(NH_4)_2SO_4$ and KCl at 25 °C, and the measured values differed from the actual values by <1% RH.

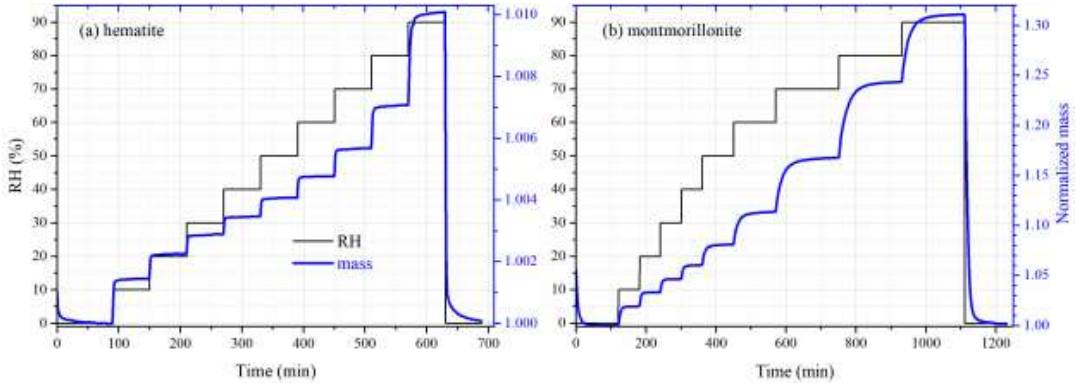


**Figure 2.** RH (black curve, left *y*-axis) and mass of mineral dust (normalized to that at <1% RH, blue curve, right *y*-axis) as a function of experimental time: (a) hematite; (b) montmorillonite.

In this work, the initial masses of mineral dust samples used typically ranged from 5 to 15 mg. As displayed in Figure 2, the sample under investigation was first dried at <1% RH; after that, RH was increased in a stepwise manner to 90%, and at each step RH was increased by 10%; at last, the sample was dried again at <1% RH. At each step we changed the RH only after the samples mass became stable, and the sample mass was considered to be stable when the mass change was <0.05% in 30 min. All the experiments were carried out in triplicate at 25 °C.

# 3 Results

## 3.1 Sample characteristics

As shown in Table 1, the BET surface areas were found to vary between 2.17±0.01 (microcline) and 249.91±0.42 $m^2/g$ (montmorillonite), spanning over two orders of magnitude. Except for montmorillonite, the BET surface areas were in the range of a few to tens of $m^2/g$. In

https://doi.org/10.5194/acp-2020-442
Preprint. Discussion started: 25 May 2020
© Author(s) 2020. CC BY 4.0 License.

Atmospheric Chemistry and Physics Discussions

addition, the average particle diameters ($d_p$) were determined to range from 0.80 μm (hematite) to 54.41 μm (M'Bour dust), and their size distributions can be found in Figures S1-S7.

Tables S1-S2 show mass fractions of water soluble inorganic ions for the twenty one mineral dust samples considered in this study. $Na^+$, $K^+$, $Ca^{2+}$, $Mg^{2+}$, $F^-$, $Cl^-$ and $SO_4^{2-}$ were detected in most of the samples, while $NH_4^+$ was above its detection limit only for two samples. The total mass fractions of all the soluble inorganic ions were found to be quite low, ranging from 0.16 mg/g for $SiO_2$ and 12.55 mg/g for Bordj dust.

**3.2 Water uptake by different mineral dust**

As described in Section 2.3, sample mass of mineral dust was measured at different RH in our work; therefore, the mass ratio of adsorbed water to the dry mineral, $m_w/m_0$, could then be determined as a function of RH. Furthermore, $m_w/m_0$ could be converted to surface coverage of adsorbed water ($\theta$), using Eq. (1) (Tang et al., 2016):

$$\theta = \frac{m_w}{m_0} \cdot \frac{N_A \cdot A_w}{M_w \cdot A_{BET}} \qquad (1),$$

where $N_A$ is Avogadro constant ($6.02\times10^{23}$ $mol^{-1}$), $M_w$ is the molar mass of water (18 g $mol^{-1}$), $A_w$ is the surface area each adsorbed water molecule would occupy (assumed to be $1\times10^{-15}$ $cm^{-2}$), and $A_{BET}$ is the BET surface (in $cm^2$ $g^{-1}$) of the mineral dust under consideration. Tables 2-5 summarize $m_w/m_0$ and $\theta$ as a function of RH for all the mineral dust examined in our work. Please note that our previous work (Tang et al., 2019c) discussed water uptake by China loess and QH dust, and these results are included here to compare with the other nineteen mineral dust samples.

**Table 2.** Mass ratios of adsorbed water to the dry mineral ($m_w/m_0$) and surface coverages of adsorbed water ($\theta$) as a function of RH (%) for $SiO_2$, $TiO_2$, magnetite, hematite, goethite and potassium feldspar.

https://doi.org/10.5194/acp-2020-442
Preprint. Discussion started: 25 May 2020
© Author(s) 2020. CC BY 4.0 License.

Atmospheric Chemistry and Physics Discussions

| RH | $SiO_2$ | | $TiO_2$ | | hematite | |
|---|---|---|---|---|---|---|
| | $m_w/m_0$ | $\theta$ | $m_w/m_0$ | $\theta$ | $m_w/m_0$ | $\theta$ |
| 10 | 0.0005±0.0001 | 0.25±0.02 | 0.0031±0.0011 | 0.19±0.07 | 0.0014±0.0001 | 0.52±0.02 |
| 20 | 0.0008±0.0001 | 0.40±0.05 | 0.0054±0.0012 | 0.33±0.07 | 0.0022±0.0001 | 0.81±0.03 |
| 30 | 0.0011±0.0001 | 0.55±0.05 | 0.0072±0.0012 | 0.44±0.07 | 0.0029±0.0001 | 1.03±0.04 |
| 40 | 0.0014±0.0001 | 0.70±0.05 | 0.0089±0.0012 | 0.54±0.07 | 0.0034±0.0002 | 1.24±0.06 |
| 50 | 0.0017±0.0001 | 0.86±0.06 | 0.0108±0.0012 | 0.66±0.08 | 0.0040±0.0002 | 1.46±0.07 |
| 60 | 0.0020±0.0001 | 1.04±0.07 | 0.0135±0.0013 | 0.82±0.08 | 0.0047±0.0002 | 1.72±0.07 |
| 70 | 0.0026±0.0002 | 1.32±0.09 | 0.0168±0.0013 | 1.03±0.08 | 0.0057±0.0002 | 2.06±0.07 |
| 80 | 0.0035±0.0003 | 1.81±0.14 | 0.0218±0.0013 | 1.34±0.08 | 0.0071±0.0002 | 2.56±0.07 |
| 90 | 0.0058±0.0007 | 2.95±0.35 | 0.0355±0.0013 | 2.17±0.08 | 0.0101±0.0002 | 3.68±0.08 |
| RH | goethite | | magnetite | | potassium feldspar | |
| | $m_w/m_0$ | $\theta$ | $m_w/m_0$ | $\theta$ | $m_w/m_0$ | $\theta$ |
| 10 | 0.0013±0.0001 | 0.33±0.02 | 0.0005±0.0001 | 0.27±0.01 | 0.0006±0.0001 | 0.54±0.01 |
| 20 | 0.0022±0.0002 | 0.55±0.04 | 0.0007±0.0001 | 0.39±0.07 | 0.0010±0.0001 | 0.84±0.01 |
| 30 | 0.0029±0.0002 | 0.73±0.06 | 0.0010±0.0001 | 0.52±0.08 | 0.0015±0.0003 | 1.24±0.25 |
| 40 | 0.0037±0.0005 | 0.92±0.12 | 0.0012±0.0001 | 0.64±0.07 | 0.0017±0.0003 | 1.46±0.25 |
| 50 | 0.0044±0.0005 | 1.10±0.12 | 0.0015±0.0001 | 0.77±0.07 | 0.0020±0.0003 | 1.70±0.24 |
| 60 | 0.0052±0.0005 | 1.30±0.12 | 0.0018±0.0001 | 0.93±0.07 | 0.0023±0.0002 | 1.92±0.17 |
| 70 | 0.0061±0.0004 | 1.53±0.11 | 0.0022±0.0001 | 1.15±0.07 | 0.0027±0.0002 | 2.25±0.17 |
| 80 | 0.0075±0.0004 | 1.88±0.10 | 0.0029±0.0001 | 1.55±0.04 | 0.0035±0.0002 | 2.92±0.19 |
| 90 | 0.0124±0.0004 | 3.09±0.11 | 0.0052±0.0003 | 2.72±0.16 | 0.0056±0.0003 | 4.73±0.21 |

Below we discuss hygroscopicity of mineral dust investigated, and compare our measured $m_w/m_0$ and $\theta$ with those reported in previous work. As our work directly measured mass change of mineral dust due to water uptake, we prefer to compare $m_w/m_0$ when such values were also reported in previous studies; otherwise, we then choose to compare $\theta$. As aerosol-based measurements are usually not sensitive enough and also need the particle sphericity assumption (Tang et al., 2016), we do not compare our results with those measurements.

https://doi.org/10.5194/acp-2020-442
Preprint. Discussion started: 25 May 2020
© Author(s) 2020. CC BY 4.0 License.

Atmospheric Chemistry and Physics Discussions

206 **3.2.1 $SiO_2$ and $TiO_2$**

207 In our work $m_w/m_0$ was determined to be 0.0011, 0.0020 and 0.0058 for $SiO_2$ at 30%, 60%
208 and 90% RH, corresponding to $\theta$ of 0.55, 1.04 and 2.95, respectively. Figure 3a compares our work
209 with previous studies in which FTIR (Goodman et al., 2001; Ma et al., 2010a; Joshi et al., 2017)
210 and QCM (Schuttlefield et al., 2007a; Yeşilbaş and Boily, 2016) were used to measure water
211 uptake by $SiO_2$. At a given RH, $\theta$ values reported by the four previous studies (Goodman et al.,
212 2001; Schuttlefield et al., 2007a; Ma et al., 2010a; Joshi et al., 2017) were generally larger than
213 our work, and the difference usually did not exceed a factor of three. Furthermore, the differences
214 between our work and the four previous studies became smaller at higher RH. For example, at 80%
215 RH our measured $\theta$ was very close to those reported by Ma et al. (2010a) and Joshi et al. (2017),
216 and at 90% RH our measured $\theta$ was 20-30% larger than those reported by the two studies (Ma et
217 al., 2010a; Joshi et al., 2017). Yeşilbaş and Boily (2016) employed a QCM to investigate water
218 adsorption on quartz (0.3-14 μm), and $\theta$ was determined to be ~2300 at ~70% RH, almost three
219 orders of magnitude larger than these reported in our work and other previous studies (Goodman
220 et al., 2001; Schuttlefield et al., 2007a; Ma et al., 2010a; Joshi et al., 2017); therefore, the results
221 reported by Yeşilbaş and Boily (2016) are not included in Figure 3a.

https://doi.org/10.5194/acp-2020-442
Preprint. Discussion started: 25 May 2020
© Author(s) 2020. CC BY 4.0 License.

Atmospheric Chemistry and Physics Discussions

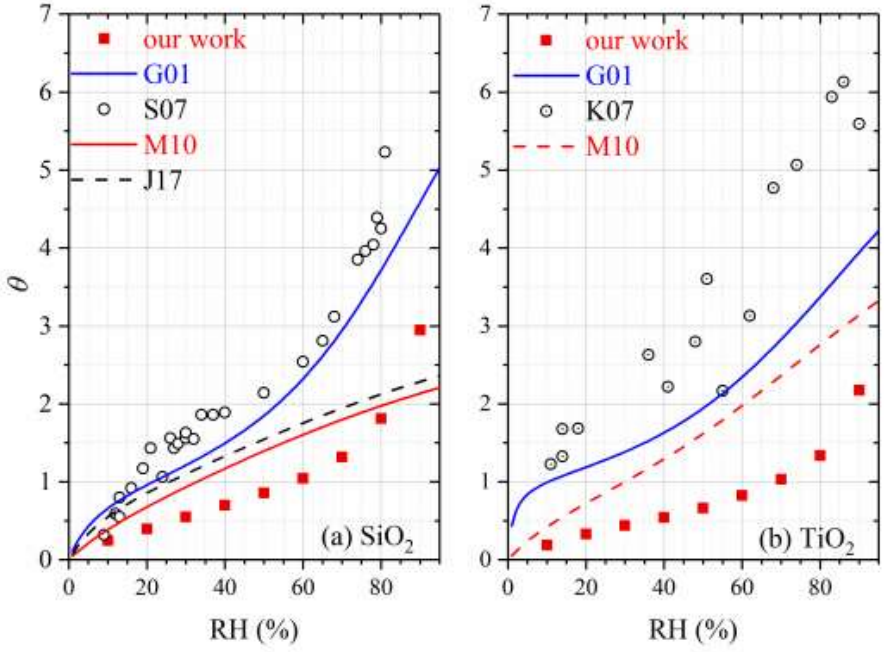


222

223 **Figure 3.** Comparison of surface coverages of adsorbed water ($\theta$) measured in our work with those
224 reported in previous studies for (a) $SiO_2$ and (b) $TiO_2$. G01: Goodman et al. (2001); S07:
225 Schuttlefield et al. (2007a); M10: Ma et al. (2010a); J17: Joshi et al. (2017); K07: Ketteler et al.
226 (2007).

227

228 For $TiO_2$, $m_w/m_0$ was determined to be 0.0072, 0.0135 and 0.0355 at 30%, 60% and 90%
229 RH, corresponding to $\theta$ of 0.44, 0.82 and 2.17, respectively. Water adsorption on P25 $TiO_2$ was
230 studied previously using FTIR (Goodman et al., 2001; Ma et al., 2010a), and another study
231 (Ketteler et al., 2007) employed atmospheric pressure X-ray photoelectron spectroscopy to explore
232 interactions of water vapor with the rutile single crystal surface (110). As shown in Figure 3b,
233 when compared with our work, $\theta$ values reported by Ma et al. (2010a) were higher across the entire
234 RH range, and the relative differences between our work and Ma et al. (2010a) were around a

https://doi.org/10.5194/acp-2020-442
Preprint. Discussion started: 25 May 2020
© Author(s) 2020. CC BY 4.0 License.

Atmospheric Chemistry and Physics Discussions

factor of two or smaller. The relative differences between our work and the other two studies (Goodman et al., 2001; Ketteler et al., 2007) were larger, being a factor of ~5 at lower RH and becoming smaller at higher RH.

### 3.2.2 Hematite, goethite and magnetite

At 30%, 60% and 90% RH, $m_w/m_0$ was measured to be 0.0029, 0.0047 and 0.0101 for hematite, corresponding to $\theta$ of 1.03, 1.72 and 3.68. Water adsorption on hematite was studied previously using FTIR (Goodman et al., 2001; Ma et al., 2010a) and QCM (Yeşilbaş and Boily, 2016). Figure 4a reveals that our results agreed reasonably well with those reported by Goodman et al. (2001) and Ma et al. (2010a), and the relative differences were found to be within a factor of two. In addition, our results agreed fairly well with those reported for 10 nm hematite by Yeşilbaş and Boily (2016), but were significantly smaller than their results for 50 nm hematite. Yeşilbaş and Boily (2016) also studied water adsorption on 4 and 5 μm hematite particles, and $\theta$ were reported to be ~300 at ~70% RH, almost two orders of magnitude larger than our results; therefore, their measured $\theta$ for 4 and 5 μm hematite are not shown in Figure 4a.

In our work, $m_w/m_0$ was measured to be 0.0029, 0.0052 and 0.0124 at 30%, 60% and 90% RH for goethite, corresponding to $\theta$ of 0.73, 1.30 and 3.09. Yeşilbaş and Boily (2016) employed QCM to study water adsorption on goethite, and their measured $\theta$ are plotted in Figure 4b to compare ours. Compared to our work, on average $\theta$ values measured by Yeşilbaş and Boily (2016) were a factor of ~2 larger. We also investigated water adsorption on magnetite, and the results can be found in Figure 4b. Compared to goethite, $\theta$ values were generally 20-30% smaller for magnetite. As far as we know, water adsorption on magnetite was not quantitatively investigated before.

https://doi.org/10.5194/acp-2020-442
Preprint. Discussion started: 25 May 2020
© Author(s) 2020. CC BY 4.0 License.

Atmospheric Chemistry and Physics Discussions

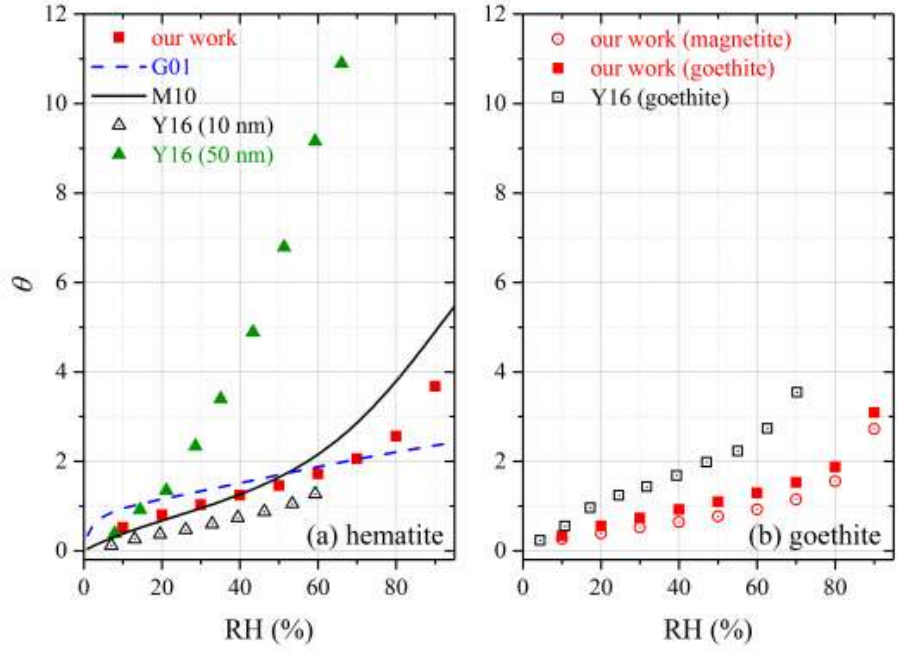


**Figure 4.** Comparison of surface coverages of adsorbed water ($\theta$) measured in our work with those reported in previous studies for (a) hematite and (b) goethite ($\theta$ measured in our work for magnetite are also plotted). G01: Goodman et al. (2001); M10: Ma et al. (2010a); Y16, Yeşilbaş and Boily (2016).

### 3.2.3 Feldspars

Tables 2-3 show that $m_w/m_0$ were determined to be 0.0056, 0.0060 and 0.0048 at 90% RH for potassium feldspar, albite and microcline, respectively; correspondingly, $\theta$ were found to be 4.73, 5.53 and 7.37. QCM was used by Yeşilbaş and Boily (2016) to study water uptake onto microcline, and $\theta$ was measured to be ~300 at ~70% RH, about two orders of magnitude larger than our results. We are not aware of other previous studies which investigated water adsorption on feldspars in a quantitative manner.

https://doi.org/10.5194/acp-2020-442
Preprint. Discussion started: 25 May 2020
© Author(s) 2020. CC BY 4.0 License.

Atmospheric Chemistry and Physics Discussions

**Table 3.** Mass ratios of adsorbed water to the dry mineral ($m_w/m_0$) and surface coverages of adsorbed water ($\theta$) as a function of RH (%) for albite, microcline, $CaCO_3$, dolomite, illite and kaolinite.

| RH | albite | | microcline | | $CaCO_3$ | |
|---|---|---|---|---|---|---|
| | $m_w/m_0$ | $\theta$ | $m_w/m_0$ | $\theta$ | $m_w/m_0$ | $\theta$ |
| 10 | 0.0007±0.0002 | 0.67±0.20 | 0.0003±0.0001 | 0.51±0.10 | 0.0001±0.0001 | 0.10±0.07 |
| 20 | 0.0011±0.0002 | 1.00±0.19 | 0.0005±0.0001 | 0.81±0.14 | 0.0002±0.0002 | 0.27±0.24 |
| 30 | 0.0013±0.0001 | 1.19±0.04 | 0.0007±0.0001 | 1.06±0.19 | 0.0002±0.0002 | 0.38±0.28 |
| 40 | 0.0016±0.0001 | 1.45±0.04 | 0.0008±0.0002 | 1.28±0.26 | 0.0002±0.0001 | 0.33±0.17 |
| 50 | 0.0019±0.0001 | 1.74±0.04 | 0.0010±0.0002 | 1.57±0.29 | 0.0003±0.0001 | 0.41±0.22 |
| 60 | 0.0023±0.0001 | 2.10±0.03 | 0.0014±0.0002 | 2.11±0.30 | 0.0004±0.0002 | 0.63±0.31 |
| 70 | 0.0028±0.0001 | 2.63±0.05 | 0.0019±0.0001 | 2.96±0.22 | 0.0005±0.0002 | 0.79±0.34 |
| 80 | 0.0038±0.0001 | 3.50±0.06 | 0.0028±0.0002 | 4.40±0.33 | 0.0007±0.0003 | 1.02±0.39 |
| 90 | 0.0060±0.0001 | 5.53±0.06 | 0.0048±0.0006 | 7.37±0.98 | 0.0011±0.0005 | 1.73±0.79 |
| RH | dolomite | | illite | | kaolinite | |
| | $m_w/m_0$ | $\theta$ | $m_w/m_0$ | $\theta$ | $m_w/m_0$ | $\theta$ |
| 10 | 0.0004±0.0001 | 0.13±0.02 | 0.0050±0.0001 | 0.69±0.01 | 0.0014±0.0003 | 0.48±0.10 |
| 20 | 0.0007±0.0001 | 0.21±0.02 | 0.0083±0.0001 | 1.15±0.01 | 0.0024±0.0004 | 0.83±0.14 |
| 30 | 0.0009±0.0001 | 0.26±0.04 | 0.0110±0.0001 | 1.53±0.01 | 0.0032±0.0005 | 1.12±0.17 |
| 40 | 0.0011±0.0002 | 0.31±0.05 | 0.0135±0.0002 | 1.88±0.03 | 0.0040±0.0006 | 1.38±0.20 |
| 50 | 0.0013±0.0002 | 0.36±0.06 | 0.0157±0.0002 | 2.18±0.03 | 0.0047±0.0007 | 1.63±0.23 |
| 60 | 0.0015±0.0002 | 0.42±0.06 | 0.0181±0.0005 | 2.52±0.07 | 0.0056±0.0008 | 1.95±0.27 |
| 70 | 0.0018±0.0003 | 0.51±0.08 | 0.0210±0.0007 | 2.93±0.09 | 0.0070±0.0009 | 2.43±0.32 |
| 80 | 0.0025±0.0005 | 0.70±0.15 | 0.0253±0.0007 | 3.52±0.10 | 0.0093±0.0010 | 3.22±0.36 |
| 90 | 0.0045±0.0005 | 1.26±0.14 | 0.0333±0.0007 | 4.63±0.10 | 0.0146±0.0011 | 5.08±0.39 |

### 3.2.4 Carbonates

https://doi.org/10.5194/acp-2020-442
Preprint. Discussion started: 25 May 2020
© Author(s) 2020. CC BY 4.0 License.

Atmospheric Chemistry and Physics Discussions

The mass ratio of adsorbed water to the dry mineral, $m_w/m_0$, was measured in our work to be 0.0011 at 90% RH for $CaCO_3$, giving a $\theta$ value of 1.73. Water adsorption on $CaCO_3$ was investigated previously, using thermogravimetric analysis (Gustafsson et al., 2005), physisorption analysis (Ma et al., 2012a) and QCM (Hatch et al., 2008; Schuttlefield, 2008; Yeşilbaş and Boily, 2016). Hatch et al. (2008) and Ma et al. (2008) reported $m_w/m_0$ as a function of RH; Figure 5a shows that compared to our work, $m_w/m_0$ values determined by Hatch et al. (2008) were significantly larger (by a factor of 10 or more), whereas the results reported by Ma et al. (2012) were smaller by a factor of ~2. We further compare our measured $\theta$ with those reported by another two studies (Gustafsson et al., 2005; Schuttlefield, 2008). As shown in Figure 5b, the results reported by Gustafsson et al. (2005) and Schuttlefield (2008) were found to be larger than ours, by a factor of 2-3. In addition, $\theta$ was measured to be >100 at ~70% RH for $CaCO_3$ (Yeşilbaş and Boily, 2016), approximately two orders of magnitude larger than our work.

As shown in Table 3, our work suggested that around 1.26 monolayers of adsorbed water was formed on dolomite at 90% RH, similar to that for $CaCO_3$. To our knowledge, water adsorption on dolomite has not been quantitatively explored by previous work.

https://doi.org/10.5194/acp-2020-442
Preprint. Discussion started: 25 May 2020
© Author(s) 2020. CC BY 4.0 License.

Atmospheric Chemistry and Physics Discussions

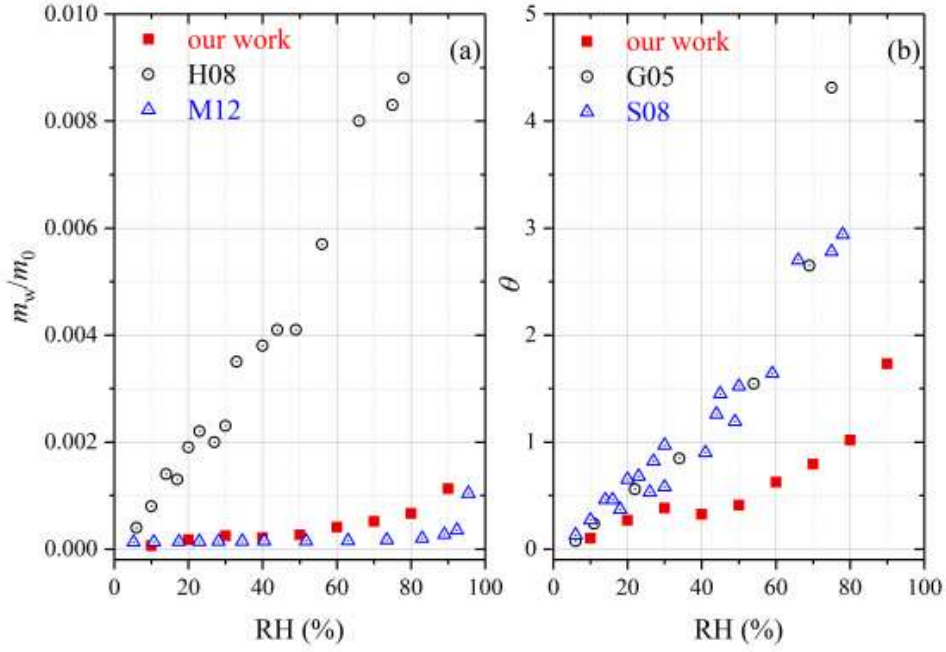


**Figure 5.** Comparison of water adsorption on $CaCO_3$ examined in different studies: (a) mass ratios of adsorbed water to the dry mineral ($m_w/m_0$); (b) surface coverages of adsorbed water ($\theta$). G05, Gustafsson et al. (2005); H08, Hatch et al. (2008); S08, Schuttlefield (2008); M12, Ma et al. (2012).

### 3.2.5 Clay minerals

For illite, $m_w/m_0$ and $\theta$ were determined to be 0.0333 and 4.63 at 90% RH in our study. QCM was employed to study water adsorption on illite, and $m_w/m_0$ was reported to be 0.28 at ~90% RH (Hatch et al., 2011) and ~0.27 at 75% RH (Schuttlefield et al., 2007b), around one order of magnitude larger than our results. A recent study (Yeşilbaş and Boily, 2016) also investigated water uptake onto illite using QCM, and their reported $\theta$ are compared with our results in Figure 6a. The relative differences between our and their (Yeşilbaş and Boily, 2016) work were usually smaller than a factor of two, and became even smaller at higher RH.

https://doi.org/10.5194/acp-2020-442
Preprint. Discussion started: 25 May 2020
© Author(s) 2020. CC BY 4.0 License.

Atmospheric Chemistry and Physics Discussions

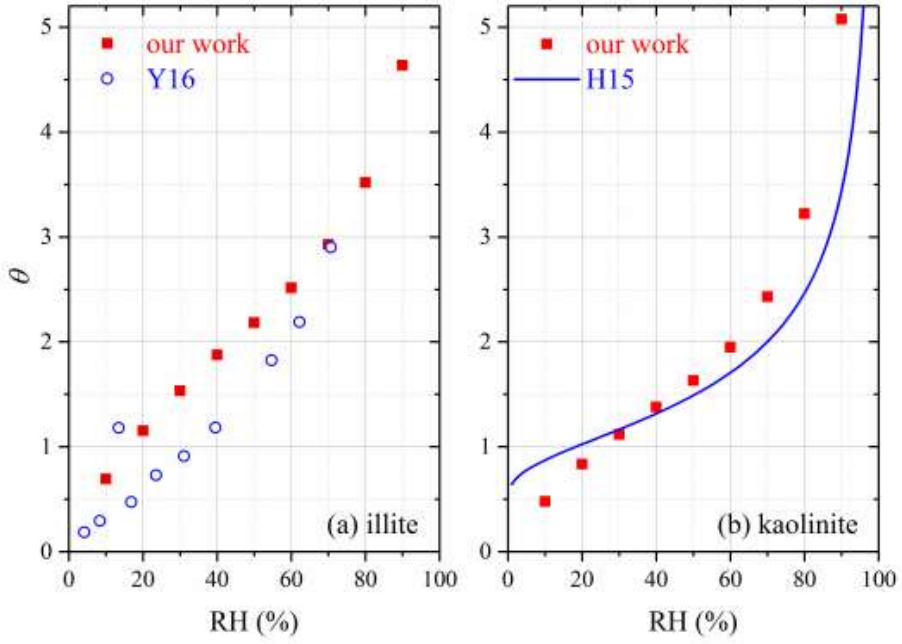


305

306 **Figure 6.** Comparison of surface coverages of adsorbed water ($\theta$) measured by different studies
307 for (a) illite and (b) kaolinite. H15, Hung et al. (2015); Y16, Yeşilbaş and Boily (2016).

308

309 For kaolinite, $m_w/m_0$ and $\theta$ were determined in our work to 0.0093 and 3.22 at 80% RH and
310 0.0146 and 5.08 at 90% RH, respectively. A few previous studies investigated water adsorption on
311 kaolinite using QCM (Schuttlefield et al., 2007b; Hatch et al., 2011; Yeşilbaş and Boily, 2016)
312 and physisorption analysis (Hung et al., 2015). Figure 6b compares our measured $\theta$ with those
313 reported by Hung et al. (2015), suggesting that the two studies were in good agreement, and the
314 relative differences were usually within 30%. At ~80% RH, $m_w/m_0$ were determined to be ~0.03
315 for kaolinite provided by Alfa and ~0.1 for kaolinite (KGa-1b) obtained from Clay Mineral Society
316 (Schuttlefield et al., 2007b), around three and ten times larger than our work. In the work by Hatch
317 et al. (2011), $m_w/m_0$ was determined to be ~0.1 at ~80% RH for kaolinite (KGa-1b), about one

https://doi.org/10.5194/acp-2020-442
Preprint. Discussion started: 25 May 2020
© Author(s) 2020. CC BY 4.0 License.

Atmospheric Chemistry and Physics Discussions

318 order of magnitude larger than our result. Yeşilbaş and Boily (2016) examined water adsorption
319 on two different kaolinite samples (kaolinite provided by Fluka and KGa-1), and $\theta$ were found to
320 be up to 100 at ~70% RH, being >30 times larger than our work.

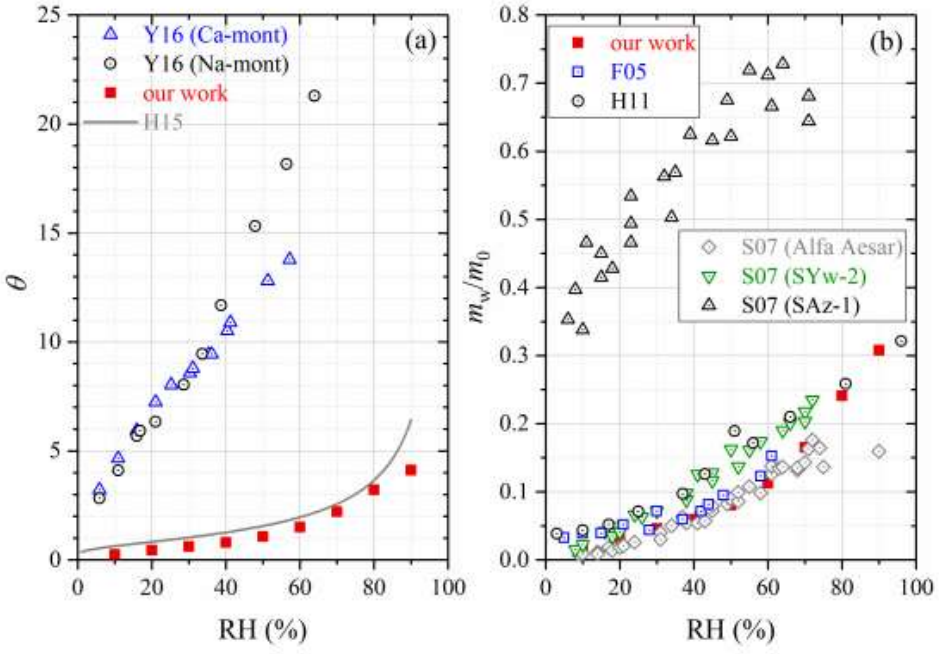


321

322 **Figure 7.** Comparison of water adsorption on montmorillonite examined in different studies: (a)
323 surface coverages of adsorbed water ($\theta$); (b) the mass ratio of adsorbed water to the dry mineral
324 ($m_w/m_0$). F05, Frinak et al. (2005); S07, Schuttlefield et al. (2007); H11, Hatch et al. (2011); H15,
325 Hung et al. (2015); Y16, Yeşilbaş and Boily (2016).

326

327 We also studied water adsorption on montmorillonite, and $m_w/m_0$ and $\theta$ were measured to
328 be 0.308 and 4.12 at 90% RH. Physisorption analysis (Hung et al., 2015) and QCM (Yeşilbaş and
329 Boily, 2016) were utilized to investigate water uptake onto montmorillonite. As shown in Figure
330 7a, our work agreed well with Hung et al. (2015), and the results obtained by Yeşilbaş and Boily

https://doi.org/10.5194/acp-2020-442
Preprint. Discussion started: 25 May 2020
© Author(s) 2020. CC BY 4.0 License.

Atmospheric Chemistry and Physics Discussions

(2016) for Ca- and Na-montmorillonite were much larger (by a factor of >10), when compared with our work. Figure 7b compares our measured $m_w/m_0$ with those reported in previous studies in which FTIR (Frinak et al., 2005) and QCM (Schuttlefield et al., 2007b; Hatch et al., 2011) were used. In general good agreement between our work and the three previous studies were found, except for SAz-1 montmorillonite (Schuttlefield et al., 2007b). One possible explanation for the observed discrepancy is that montmorillonite samples from different sources may have different hygroscopic properties. We note that prior to 2005, a few studies (Hall and Astill, 1989; Cases et al., 1992; Xu et al., 2000; Zent et al., 2001) also investigated water uptake by montmorillonite, and it was found that these studies agreed well with Frinak et al. (2005); therefore, the four studies conducted before 2005 should also be consistent with our work.

In addition, water uptake by chlorite was explored in our work. As shown in Table 4, $m_w/m_0$ and $\theta$ were measured to be 0.012 and 4.03 at 90% RH. To our knowledge, hygroscopic properties of chlorite have not been examined before.

**Table 4.** Mass ratio of adsorbed water to the dry mineral ($m_w/m_0$) and surface coverages of adsorbed water ($\theta$) as a function of RH (%) for montmorillonite, chlorite, ATD, M'Bour dust, Bordj dust and Saharan dust.

| RH | montmorillonite | | chlorite | | ATD | |
|---|---|---|---|---|---|---|
| | $m_w/m_0$ | $\theta$ | $m_w/m_0$ | $\theta$ | $m_w/m_0$ | $\theta$ |
| 10 | 0.0192±0.0002 | 0.26±0.01 | 0.0013±0.0001 | 0.42±0.02 | 0.0099±0.0001 | 0.90±0.01 |
| 20 | 0.0333±0.0003 | 0.45±0.01 | 0.0021±0.0001 | 0.70±0.03 | 0.0161±0.0002 | 1.47±0.02 |
| 30 | 0.0463±0.0004 | 0.62±0.01 | 0.0028±0.0001 | 0.94±0.04 | 0.0209±0.0001 | 1.91±0.01 |
| 40 | 0.0597±0.0008 | 0.80±0.01 | 0.0034±0.0001 | 1.14±0.04 | 0.0253±0.0001 | 2.31±0.01 |
| 50 | 0.0802±0.0009 | 1.07±0.01 | 0.0040±0.0001 | 1.34±0.05 | 0.0296±0.0001 | 2.70±0.01 |
| 60 | 0.1125±0.0011 | 1.51±0.02 | 0.0047±0.0001 | 1.57±0.05 | 0.0341±0.0001 | 3.11±0.01 |
| 70 | 0.1654±0.0023 | 2.21±0.03 | 0.0057±0.0001 | 1.93±0.05 | 0.0394±0.0001 | 3.59±0.01 |

https://doi.org/10.5194/acp-2020-442
Preprint. Discussion started: 25 May 2020
© Author(s) 2020. CC BY 4.0 License.

Atmospheric Chemistry and Physics Discussions

| | | | | | | |
|---|---|---|---|---|---|---|
| 80 | 0.2407±0.0025 | 3.22±0.03 | 0.0077±0.0001 | 2.57±0.05 | 0.0470±0.0003 | 4.29±0.03 |
| 90 | 0.3080±0.0029 | 4.12±0.04 | 0.0120±0.0002 | 4.03±0.08 | 0.0644±0.0009 | 5.87±0.08 |

| RH | M'Bour dust | | Bordj dust | | Saharan dust | |
|---|---|---|---|---|---|---|
| | $m_w/m_0$ | $\theta$ | $m_w/m_0$ | $\theta$ | $m_w/m_0$ | $\theta$ |
| 10 | 0.0014±0.0001 | 0.31±0.01 | 0.0010±0.0001 | 0.21±0.01 | 0.0102±0.0002 | 0.66±0.02 |
| 20 | 0.0023±0.0001 | 0.54±0.01 | 0.0020±0.0005 | 0.41±0.09 | 0.0166±0.0004 | 1.02±0.03 |
| 30 | 0.0032±0.0001 | 0.73±0.02 | 0.0026±0.0005 | 0.53±0.09 | 0.0214±0.0002 | 1.39±0.01 |
| 40 | 0.0039±0.0003 | 0.90±0.07 | 0.0034±0.0004 | 0.69±0.08 | 0.0260±0.0002 | 1.69±0.01 |
| 50 | 0.0046±0.0004 | 1.06±0.10 | 0.0040±0.0004 | 0.82±0.08 | 0.0304±0.0003 | 1.98±0.02 |
| 60 | 0.0052±0.0005 | 1.21±0.13 | 0.0050±0.0004 | 1.02±0.09 | 0.0360±0.0002 | 2.34±0.02 |
| 70 | 0.0069±0.0006 | 1.59±0.13 | 0.0076±0.0005 | 1.55±0.10 | 0.0438±0.0003 | 2.84±0.02 |
| 80 | 0.0092±0.0006 | 2.13±0.14 | 0.0118±0.0004 | 2.41±0.08 | 0.0557±0.0007 | 3.62±0.05 |
| 90 | 0.0152±0.0005 | 3.51±0.11 | 0.0192±0.0003 | 3.91±0.07 | 0.0793±0.0015 | 5.15±0.10 |

### 3.2.6 Authentic mineral dust

**ATD:** Table 4 suggests that at 90% RH, $m_w/m_0$ and $\theta$ were measured in our work to be 0.0644 and 5.87 for ATD. Two previous studies (Navea et al., 2010; Yeşilbaş and Boily, 2016) employed QCM to investigate water adsorption on ATD. In the first study (Navea et al., 2010), $m_w/m_0$ was measured to be >0.1 at 70% RH, being 2-3 times larger than our result (~0.04 at 70% RH); in the second study (Yeşilbaş and Boily, 2016), $\theta$ was measured to be >200 at ~70% RH, almost two orders of magnitude larger than our work (~3.6 at 70% RH). Gustafsson et al. (2005) used a thermogravimetric analyzer to study water uptake by ATD, and as shown in Figure 8a, their results agreed very well with ours. A recent study (Joshi et al., 2017) investigated water adsorption on ATD using FTIR; compared to our work, the values reported by Joshi et al. (2017) were ~30% lower, suggesting fairly good agreement between the two studies.

https://doi.org/10.5194/acp-2020-442
Preprint. Discussion started: 25 May 2020
© Author(s) 2020. CC BY 4.0 License.

Atmospheric Chemistry and Physics Discussions

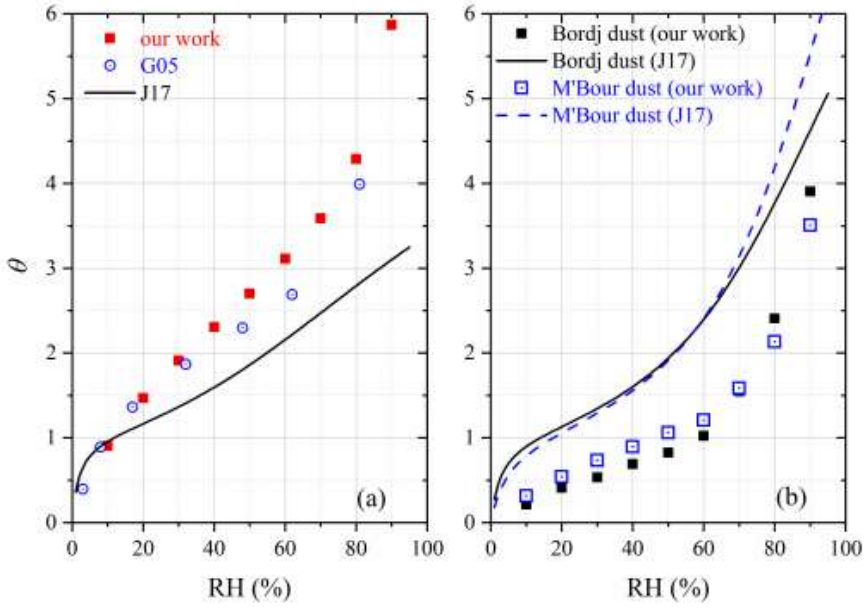


**Figure 8.** Comparison of surface coverages of adsorbed water ($\theta$) reported in different studies for (a) ATD and (b) Bordj dust and M'Bour dust. G05, Gustafsson et al. (2005); J17, Joshi et al. (2017).

**African dust:** In our study, $m_w/m_0$ and $\theta$ were measured to be 0.0192 and 3.91 for Bordj dust and 0.0152 and 3.51 for M'Bour dust at 90% RH. Joshi et al. (2017) employed FTIR to investigate interaction of water vapor with Bordj dust and M'Bour dust. As suggested by Figure 8b, the relative differences between our and their work (Joshi et al., 2017) were usually within a factor of two for the two dust samples, and the discrepancy also became smaller at higher RH, suggesting fair consistence between the two studies.

For Saharan dust, $m_w/m_0$ and $\theta$ were determined in our study to be 0.0793 and 5.15 at 90% RH. Water uptake onto Saharan dust was studied using QCM (Navea et al., 2010), and their results, as shown in Figure 9a, were 2-3 times larger than our work.

https://doi.org/10.5194/acp-2020-442
Preprint. Discussion started: 25 May 2020
© Author(s) 2020. CC BY 4.0 License.

Atmospheric Chemistry and Physics Discussions

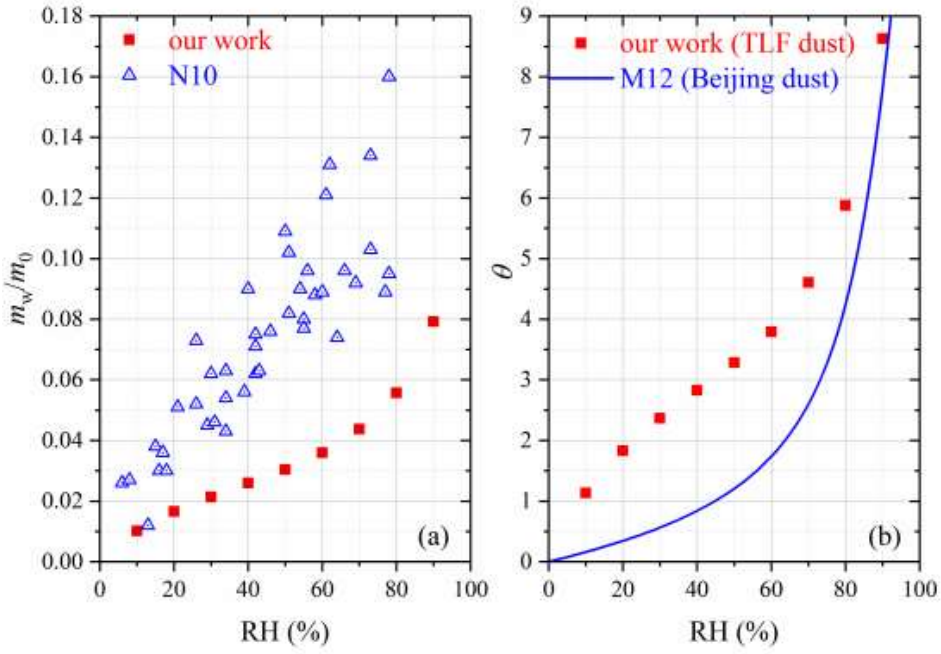


373

374 **Figure 9.** (a) Comparison of mass ratios of adsorbed water to the dry mineral ($m_w/m_0$) measured
375 by our work and N10 (Navea et al., 2010) for Saharan dust. (b) Comparison of surface coverages
376 of adsorbed water ($\theta$) for TLF dust measured in our work with Beijing dust measured by M12 (Ma
377 et al., 2012b).

378

379 **Asian dust:** Table 5 summarizes our results obtained for three Asian mineral dust samples,
380 including China loess, QH dust and TLF dust. It should be pointed out that $m_w/m_0$ have been
381 reported in our previous work (Tang et al., 2019c) for China loess and QH dust, and they are
382 included here for comparison. As shown in Table 5, the three Asian authentic dust samples
383 exhibited very similar water uptake properties, and their $m_w/m_0$ were determined to be 0.021-0.022
384 at 90% RH. Navea et al. (2010) employed QCM to study interaction of water vapor with China

https://doi.org/10.5194/acp-2020-442
Preprint. Discussion started: 25 May 2020
© Author(s) 2020. CC BY 4.0 License.

Atmospheric Chemistry and Physics Discussions

loess, and $m_w/m_0$ was reported to be ~0.17 at 70% RH, more than one order of magnitude larger than our result (~0.012 at 70% RH).

As mentioned in Section 2.1, TLF dust examined in our work were airborne dust particles collected during a dust storm in Turpan (Xinjiang, China) which was very close to the dust source. In a previous study (Ma et al., 2012b), dust particles (termed as Beijing dust here) were collected during a dust storm in Beijing (and thus these particles had undergone atmospheric aging to some extent), and their hygroscopic properties were then investigated using a physisorption analyzer. As revealed by Figure 9b, our work agreed fairly well with Ma et al. (2012b) at high RH (70%, 80% and 90%), though the differences were considerably larger at lower RH.

**Table 5.** Mass ratios of adsorbed water to the dry mineral ($m_w/m_0$) and surface coverages of adsorbed water ($\theta$) as a function of RH (%) for QH dust, China loess and TLF dust.

| RH | QH dust | | China loess | | TLF dust | |
|---|---|---|---|---|---|---|
| | $m_w/m_0$ | $\theta$ | $m_w/m_0$ | $\theta$ | $m_w/m_0$ | $\theta$ |
| 10 | 0.0022±0.0001 | 0.84±0.01 | 0.0030±0.0001 | 0.87±0.03 | 0.0029±0.0001 | 1.13±0.05 |
| 20 | 0.0037±0.0001 | 1.39±0.01 | 0.0049±0.0001 | 1.39±0.04 | 0.0047±0.0002 | 1.83±0.08 |
| 30 | 0.0049±0.0001 | 1.86±0.01 | 0.0062±0.0001 | 1.78±0.04 | 0.0060±0.0002 | 2.37±0.09 |
| 40 | 0.0060±0.0001 | 2.29±0.01 | 0.0074±0.0001 | 2.12±0.03 | 0.0072±0.0002 | 2.83±0.09 |
| 50 | 0.0072±0.0001 | 2.75±0.01 | 0.0087±0.0002 | 2.49±0.04 | 0.0083±0.0002 | 3.28±0.09 |
| 60 | 0.0086±0.0001 | 3.29±0.01 | 0.0102±0.0002 | 2.90±0.04 | 0.0096±0.0003 | 3.79±0.11 |
| 70 | 0.0104±0.0001 | 3.96±0.01 | 0.0119±0.0002 | 3.41±0.05 | 0.0117±0.0004 | 4.61±0.16 |
| 80 | 0.0134±0.0001 | 5.09±0.02 | 0.0146±0.0002 | 4.17±0.05 | 0.0149±0.0007 | 5.88±0.26 |
| 90 | 0.0215±0.0001 | 8.20±0.01 | 0.0212±0.0003 | 6.05±0.07 | 0.0219±0.0012 | 8.63±0.46 |

### 3.2.7 Discussion

To investigate water adsorption by mineral dust, one previous study (Gustafsson et al., 2005) employed thermogravimetric analysis which measured sample mass as a function of RH

https://doi.org/10.5194/acp-2020-442
Preprint. Discussion started: 25 May 2020
© Author(s) 2020. CC BY 4.0 License.

Atmospheric Chemistry and Physics Discussions

(essentially the same to VSA used in our study), and another two groups (Ma et al., 2012a; Ma et al., 2012b; Hung et al., 2015) employed physisorption analysis which measured change in water vapor pressure caused by adsorption onto mineral dust (Ma et al., 2010b). Thermogravimetric analysis, physisorption analysis and the VSA technique used in our work can be considered as absolutely quantitative, and as discussed in Section 3.2, in general our work agreed well with the four previous studies (Gustafsson et al., 2005; Ma et al., 2012a; Ma et al., 2012b; Hung et al., 2015).

FTIR was widely employed in previous work (Goodman et al., 2001; Frinak et al., 2005; Ma et al., 2010a; Joshi et al., 2017; Ibrahim et al., 2018) to study water uptake onto mineral dust, although it is not straightforward to convert IR absorption intensities of adsorbed water to its absolute amounts (Schuttlefield et al., 2007a; Ma et al., 2010b; Tang et al., 2019a). The relative differences between these studies and our work were typically within a factor of 2-3; since even for dust samples with the same name, samples examined in different studies may actually differ substantially in composition and water uptake properties, the agreement between these studies and our work can be considered as fairly good.

QCM is another technique widely used to investigate water uptake onto mineral dust (Schuttlefield et al., 2007b; Hatch et al., 2008; Schuttlefield, 2008; Navea et al., 2010; Hatch et al., 2011; Yeşilbaş and Boily, 2016). As shown in Section 3.2, though good agreement was found for some mineral dust between our work and these QCM studies, large discrepancies (up to 2-3 orders of magnitude) were frequently observed. This implies that the underlying assumptions required to convert the change in resonance frequency of the quartz crystal to the change in sample mass may not always be fulfilled, and as a result the QCM results should be used with cautions.

https://doi.org/10.5194/acp-2020-442
Preprint. Discussion started: 25 May 2020
© Author(s) 2020. CC BY 4.0 License.

Atmospheric Chemistry and Physics Discussions

For the same dust (at least with the same name), different samples with distinctive hygroscopicity may have been used in our work and previous studies, contributing to the observed discrepancies. To further understand and resolve the discrepancies identified, it will be very useful to distribute the same samples to different groups (in which various techniques would be applied to study their hygroscopic properties) and compare the results obtained. Similar strategies have already been adopted before to compare different instruments used for ice nucleation research and shown to be valuable (Hiranuma et al., 2015; DeMott et al., 2018).

### 3.3 Hygroscopicity parameterizations

It has been suggested that water adsorption and hygroscopicity of insoluble particles can be parameterized as a function of RH by several theoretical models, including 1) the Brunauer-Emmet-Teller (BET) adsorption isotherm (Goodman et al., 2001; Ma et al., 2010a; Joshi et al., 2017; Ibrahim et al., 2018), 2) the Freundlich adsorption isotherm (Hatch et al., 2011), 3) Frenkel-Halsey-Hill (FHH) adsorption isotherm (Kumar et al., 2011b; Hatch et al., 2014; Hung et al., 2015; Hatch et al., 2019) and 4) the $\kappa$-Köhler equation (Chen et al., 2019; Tang et al., 2019b). In this work we attempted to use the aforementioned four models to fit our experimental data. As shown in Figure 10 (where $SiO_2$, albite, kaolinite and TLF dust are used as examples), our work suggested that the FHH adsorption isotherm could well describe the measured hygroscopicity of mineral dust samples as a function of RH. In addition, we found that the other three parameterization methods could not fit our experimental data.

https://doi.org/10.5194/acp-2020-442
Preprint. Discussion started: 25 May 2020
© Author(s) 2020. CC BY 4.0 License.

Atmospheric Chemistry and Physics Discussions

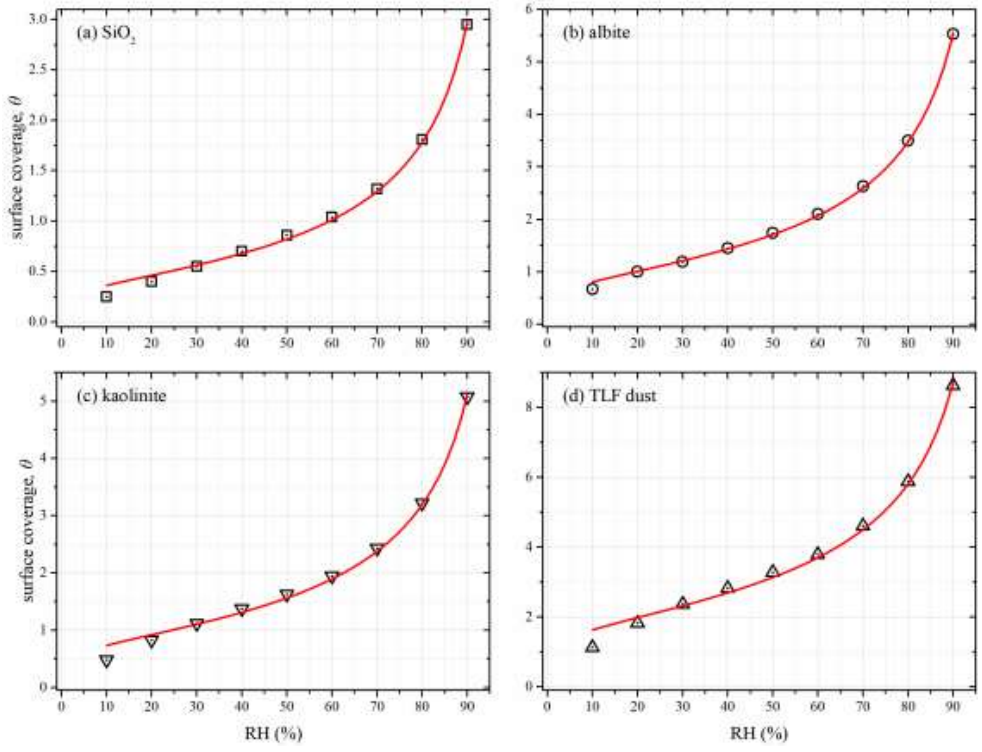


442

443 **Figure 10.** Surface coverages ($\theta$) of adsorbed water on (a) $SiO_2$, (b) albite, (c) kaolinite and (d)
444 TLF dust as a function of RH (0-90%) at 25 °C. The experimental data were fitted with Frenkel-
445 Halsey-Hill adsorption isotherm model (solid curves).

446

447 The FHH adsorption isotherm, which describes surface coverages of adsorbed water ($\theta$) as
448 a function of RH, is given by Eq. (2) (Sorjamaa and Laaksonen, 2007; Tang et al., 2016):

449 $$\theta = \sqrt[B_{FHH}]{\frac{A_{FHH}}{-\ln(RH)}} \qquad (2),$$

450 where $A_{FHH}$ and $B_{FHH}$ are empirical parameters. We found that Eq. (2) can well fit $\theta$ versus RH for
451 all the 21 mineral dust samples examined, and the generated $A_{FHH}$ and $B_{FHH}$ values are summarized
452 in Table 6. As shown in Table 6, $A_{FHH}$ values spanned from 0.15±0.01 (dolomite) to 4.39±0.81
453 (ATD), while the variation of $B_{FHH}$ was much smaller, ranging from 1.10±0.04 (for Bordj dust) to

https://doi.org/10.5194/acp-2020-442
Preprint. Discussion started: 25 May 2020
© Author(s) 2020. CC BY 4.0 License.

Atmospheric Chemistry and Physics Discussions

454 1.91±0.18 (for ATD). Our results were largely consistent with the theoretical work by Sorjamaa
455 and Laaksonen (2007), who suggested from a theoretical view that typical $A_{FHH}$ and $B_{FHH}$ values
456 should be in the range of 0.1-3.0 and 0.5-3.0.

457

458 **Table 6.** Comparison $A_{FHH}$ and $B_{FHH}$ values determined in our work for mineral dust with those
459 reported in previous studies. a: Kumar et al. (2011a); b: Hung et al. (2015); c: Hatch et al. (2019).

| sample | $A_{FHH}$ | $B_{FHH}$ | sample | $A_{FHH}$ | $B_{FHH}$ |
|---|---|---|---|---|---|
| $TiO_2$ | 0.35±0.01 | 1.52±0.05 | $SiO_2$ | 0.50±0.03 | 1.23±0.07 |
| hematite | 1.03±0.09 | 1.67±0.09 | | 2.95±0.05 [a] | 1.36±0.03 [a] |
| magnetite | 0.41±0.01 | 1.33±0.03 | $CaCO_3$ | 0.23±0.02 | 1.18±0.09 |
| goethite | 0.59±0.04 | 1.49±0.07 | | 3.00±0.04 [a] | 1.30±0.03 [a] |
| dolomite | 0.15±0.01 | 1.43±0.07 | illite | 1.96±0.23 | 1.56±0.21 |
| albite | 1.68±0.02 | 1.61±0.01 | | 1.02±0.38 [a] | 1.12±0.04 [a] |
| potassium feldspar | 1.10±0.06 | 1.42±0.09 | | 2.06 [c] | 2.19 [c] |
| microcline | 1.22±0.05 | 1.17±0.03 | kaolinite | 1.24±0.10 | 1.48±0.08 |
| chlorite | 0.96±0.06 | 1.55±0.07 | | 1.70 [b] | 2.25 [b] |
| China loess | 3.19±0.47 | 1.84±0.12 | montmorillonite | 0.65±0.05 | 1.13±0.07 |
| QH dust | 2.53±0.32 | 1.49±0.08 | | 2.06±0.72 [a] | 1.23±0.04 [a] |
| TLF dust | 4.08±0.60 | 1.59±0.12 | | 1.23±0.31 [a] | 1.08±0.03 [a] |
| Bordj dust | 0.49±0.03 | 1.10±0.04 | | 1.25 [b] | 1.33 [b] |
| M'Bour dust | 0.59±0.05 | 1.27±0.09 | | 2.28 [c] | 1.45 [c] |
| Saharan dust | 2.03±0.18 | 1.67±0.11 | ATD | 4.39±0.81 | 1.91±0.18 |
| | | | | 2.96±0.03 [a] | 1.28±0.03 [a] |

460

461 A few previous studies investigated hygroscopic properties (Hung et al., 2015; Hatch et al.,
462 2019) and CCN activities (Kumar et al., 2011b) of mineral dust, and reported $A_{FHH}$ and $B_{FHH}$ values
463 for samples they examined. Their results are also compiled in Table 6. As revealed by Table 6,
464 $B_{FHH}$ values reported in our work were reasonably consistent with previous studies, while larger
465 differences were observed for $A_{FHH}$ values. Another study (Kumar et al., 2011a) reported $A_{FHH}$ and

https://doi.org/10.5194/acp-2020-442
Preprint. Discussion started: 25 May 2020
© Author(s) 2020. CC BY 4.0 License.

Atmospheric Chemistry and Physics Discussions

466 $B_{FHH}$ values for wet-generated mineral dust aerosols. Since the hygroscopicity of wet-generated
467 mineral dust aerosols could be very different from dry-generated aerosols (Sullivan et al., 2010b;
468 Kumar et al., 2011a), the results reported by Kumar et al. (2011b) for wet-generated aerosols are
469 not further discussed.

470 ## 4 Discussions

471 As shown in Tables 2-5, among the 21 mineral dust samples examined, $m_w(90\%)/m_0$ (mass
472 ratios of adsorbed water at 90% RH to the dry sample) was found to range from 0.0011 for $CaCO_3$
473 to 0.0380 for montmorillonite, and $\theta(90\%)$ (surface coverages of adsorbed water at 90% RH)
474 varied between 1.26 for dolomite and 8.63 for TLF dust. It appears that clay minerals and authentic
475 mineral dust samples usually exhibited larger hygroscopicity on a per mass basis, when compared
476 to other mineral dust samples. $TiO_2$, for which $m_w(90\%)/m_0$ was only lower than ATD, Saharan
477 dust and montmorillonite, was an exception, probably because of its very large BET surface area
478 (54.6 $m^2\ g^{-1}$).

479 One may expect that on a per mass basis, mineral dust samples with larger surface area would
480 have larger capacities to adsorb water. This was supported by our results shown in Figure 11a,
481 which suggests that for mineral dust samples considered in our study, overall $m_w(90\%)/m_0$
482 increased with the BET surface area. Nevertheless, not all the samples obeyed this general trend,
483 indicating that other factors would also play some roles in determining the ability of mineral dust
484 to adsorb water on a per mass basis. We also explored if there was any relationship between
485 hygroscopicity of mineral dust samples and soluble materials they contained. It was found that for
486 the 21 mineral dust samples considered in our work, $m_w(90\%)/m_0$ did not show any overall
487 dependence on the amounts of soluble inorganic ions.

https://doi.org/10.5194/acp-2020-442
Preprint. Discussion started: 25 May 2020
© Author(s) 2020. CC BY 4.0 License.

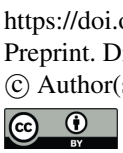

Atmospheric Chemistry and Physics Discussions

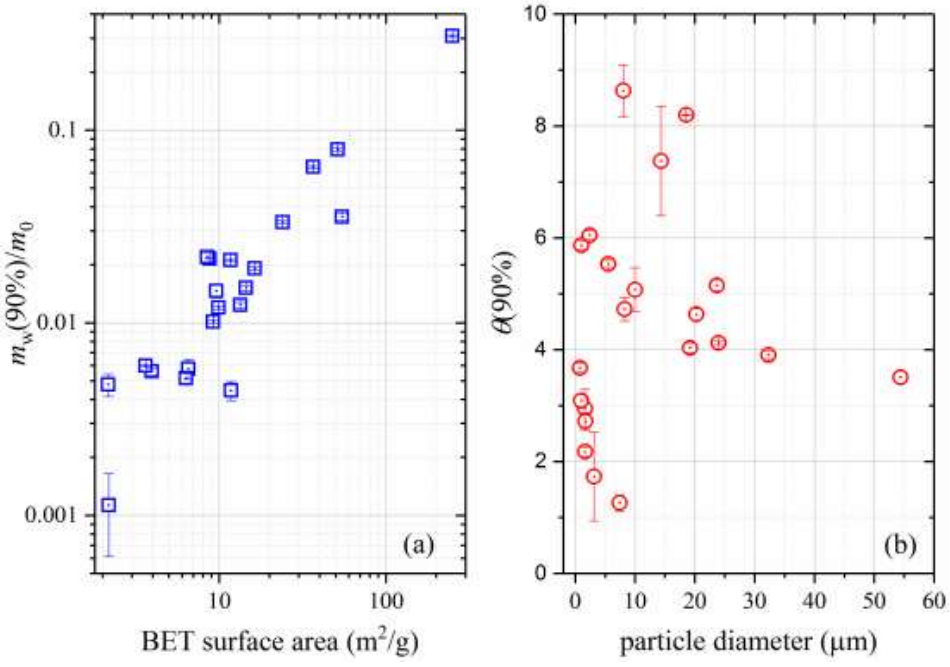


**Figure 11.** (a) The dependence of $m_w(90\%)/m_0$ (mass ratios of adsorbed water to the dry mineral at 90% RH) on BET surface areas; (b) the dependence of $\theta(90\%)$ (surface coverages of adsorbed water at 90% RH) on average particle diameters.

Ibrahim et al. (2018) studied water adsorption on ATD particles with different particle sizes, and found that the RH at which one monolayer of adsorbed water was formed increased with particle size; in other words, at the same RH the surface coverages of adsorbed water would be higher for smaller particles (Ibrahim et al., 2018). In contrast, Yeşilbaş and Boily (2016) investigated water adsorption on different mineral samples (21 in total), and suggested that at the same RH more monolayers of adsorbed water would be formed on larger particles. However, as shown in Figure 4b, our work revealed that surface coverages of adsorbed water at 90% RH showed no dependence on particle size for the 21 mineral dust samples examined in our work.

https://doi.org/10.5194/acp-2020-442
Preprint. Discussion started: 25 May 2020
© Author(s) 2020. CC BY 4.0 License.

Atmospheric Chemistry and Physics Discussions

## 5 Conclusions

Hygroscopicity largely determines environmental and climatic effects of mineral dust aerosol, one of the most abundant tropospheric aerosols. However, hygroscopic properties of mineral dust remain highly uncertain, due to relatively low hygroscopicity of mineral dust and its non-sphericity. In our work, a vapor sorption analyzer, which measured sample mass as a function of RH, was employed to investigate water adsorption and hygroscopic properties of 21 different mineral dust samples, including seven authentic mineral dust samples (from Africa, China and America) and fourteen major minerals found in tropospheric mineral dust aerosol.

For all the mineral dust samples (21 in total) examined, $m_w(90\%)/m_0$ was found to range from 0.0011 ($CaCO_3$) to 0.3080 (montmorillonite), and $\theta(90\%)$ varied between 1.26 (dolomite) and 8.63 (TLF dust). When compared to other types of mineral dust, clay minerals and authentic mineral dust samples usually exhibited larger hygroscopicity on a per mass basis. Our work suggested that overall $m_w(90\%)/m_0$ increased with the BET surface area, indicating that on a per mass basis, mineral dust samples with larger surface area would in general have larger capacities to adsorb water. Our results revealed no dependence of $m_w(90\%)/m_0$ on the amount of soluble materials contained, or no dependence of $\theta(90\%)$ on particle size. In addition, it was found in our work that the Frenkel-Halsey-Hill (FHH) adsorption isotherm could well describe surface coverages of adsorbed water as a function of RH for all the mineral dust investigated, and $A_{FHH}$ and $B_{FHH}$ parameters were determined to be in the range of 0.15-4.39 and 1.10-1.91, respectively.

**Data availability.** Data used in this paper can be found in the main text or supplement of this manuscript.

**Competing interests.** The authors declare that they have no conflict of interest.

https://doi.org/10.5194/acp-2020-442
Preprint. Discussion started: 25 May 2020
© Author(s) 2020. CC BY 4.0 License.

Atmospheric Chemistry and Physics Discussions

**Author contribution.** Mingjin Tang conceived this work; Lanxiadi Chen, Chao Peng, Wenjun Gu, Hanjing Fu and Huanhuan Zhang carried out experiments under the advice of Xing Jian and Mingjin Tang; Lanxiadi Chen, Chao Peng, Athanasios Nenes and Mingjin Tang analyzed the data and wrote the manuscript with input from all the coauthors.

**Financial support.** This work was sponsored by National Natural Science Foundation of China (91744204 and 91644106), Chinese Academy of Sciences (132744KYSB20160036), State Key Laboratory of Organic Geochemistry (SKLOG2016-A05), Guangdong Foundation for Program of Science and Technology Research (2017B030314057 and 2019B121205006), Guangdong Province (2017GC010501) and the CAS Pioneer Hundred Talents program.

**Acknowledgement.** We would like to thank John Crowley (Max Planck Institute for Chemistry, Germany) for providing Saharan dust, Pingqing Fu (Tianjin University, China) for providing TLF dust, and Manolis Romanias (Université Lille, France) for providing M'Bour dust and Bordj dust.

## Reference:

Attwood, A. R., and Greenslade, M. E.: Optical Properties and Associated Hygroscopicity of Clay Aerosols, Aerosol Sci. Technol., 45, 1350-1359, 2011.

Balkanski, Y., Schulz, M., Claquin, T., and Guibert, S.: Reevaluation of Mineral Aerosol Radiative Forcings Suggests a Better Agreement with Satellite and AERONET Data, Atmos. Chem. Phys., 7, 81-95, 2007.

Cases, J. M., Berend, I., Besson, G., Francois, M., Uriot, J. P., Thomas, F., and Poirier, J. E.: Mechanism of adsorption and desorption of water vapor by homoionic montmorillonite. 1. The sodium-exchanged form, Langmuir, 8, 2730-2739, 1992.

Chen, L. X. D., Chen, Y. Z., Chen, L. L., Gu, W. J., Peng, C., Luo, S. X., Song, W., Wang, Z., and Tang, M. J.: Hygroscopic properties of eleven pollen species in China, ACS Earth Space Chem., 3, 2678-2683, 2019.

Cziczo, D. J., Froyd, K. D., Hoose, C., Jensen, E. J., Diao, M., Zondlo, M. A., Smith, J. B., Twohy, C. H., and Murphy, D. M.: Clarifying the Dominant Sources and Mechanisms of Cirrus Cloud Formation, Science, 340, 1320-1324, 2013.

DeMott, P. J., Möhler, O., Cziczo, D. J., Hiranuma, N., Petters, M. D., Petters, S. S., Belosi, F., Bingemer, H. G., Brooks, S. D., Budke, C., Burkert-Kohn, M., Collier, K. N., Danielczok, A., Eppers, O., Felgitsch, L., Garimella, S., Grothe, H., Herenz, P., Hill, T. C. J., Höhler, K., Kanji, Z. A., Kiselev, A., Koop, T., Kristensen, T. B., Krüger, K., Kulkarni, G., Levin, E. J. T., Murray, B. J., Nicosia, A., O'Sullivan, D., Peckhaus, A., Polen, M. J., Price, H. C., Reicher, N., Rothenberg, D. A., Rudich, Y., Santachiara, G., Schiebel, T., Schrod, J., Seifried, T. M., Stratmann, F., Sullivan, R. C., Suski, K. J., Szakáll, M., Taylor, H. P., Ullrich, R., Vergara-Temprado, J., Wagner, R., Whale, T. F., Weber, D., Welti, A., Wilson, T. W., Wolf, M. J., and Zenker, J.: The Fifth International Workshop on Ice Nucleation phase 2 (FIN-02): laboratory intercomparison of ice nucleation measurements, Atmos. Meas. Tech., 11, 6231-6257, 2018.

https://doi.org/10.5194/acp-2020-442
Preprint. Discussion started: 25 May 2020
© Author(s) 2020. CC BY 4.0 License.

Atmospheric Chemistry and Physics Discussions

559 Di Biagio, C., Formenti, P., Balkanski, Y., Caponi, L., Cazaunau, M., Pangui, E., Journet, E., Nowak, S., Caquineau,
560 S., Andreae, M. O., Kandler, K., Saeed, T., Piketh, S., Seibert, D., Williams, E., and Doussin, J. F.: Global scale
561 variability of the mineral dust long-wave refractive index: a new dataset of in situ measurements for climate
562 modeling and remote sensing, Atmos. Chem. Phys., 17, 1901-1929, 2017.
563 Dupart, Y., King, S. M., Nekat, B., Nowak, A., Wiedensohler, A., Herrmann, H., David, G., Thomas, B., Miffre, A.,
564 Rairoux, P., D'Anna, B., and George, C.: Mineral dust photochemistry induces nucleation events in the presence of
565 SO2, Proc. Natl. Acad. Sci. U.S.A., 409, 20842-20847, 2012.
566 Engelbrecht, J. P., Moosmüller, H., Pincock, S., Jayanty, R. K. M., Lersch, T., and Casuccio, G.: Technical note:
567 Mineralogical, chemical, morphological, and optical interrelationships of mineral dust re-suspensions, Atmos.
568 Chem. Phys., 16, 10809-10830, 2016.
569 Formenti, P., Schutz, L., Balkanski, Y., Desboeufs, K., Ebert, M., Kandler, K., Petzold, A., Scheuvens, D.,
570 Weinbruch, S., and Zhang, D.: Recent progress in understanding physical and chemical properties of African and
571 Asian mineral dust, Atmos. Chem. Phys., 11, 8231-8256, 2011.
572 Frinak, E. K., Mashburn, C. D., Tolbert, M. A., and Toon, O. B.: Infrared characterization of water uptake by low-
573 temperature Na-montmorillonite: Implications for Earth and Mars, J. Geophys. Res.-Atmos., 110, D09308, doi:
574 09310.01029/02004JD005647, 2005.
575 Garimella, S., Huang, Y. W., Seewald, J. S., and Cziczo, D. J.: Cloud condensation nucleus activity comparison of
576 dry- and wet-generated mineral dust aerosol: the significance of soluble material, Atmos. Chem. Phys., 14, 6003-
577 6019, 2014.
578 Ginoux, P., Prospero, J. M., Gill, T. E., Hsu, N. C., and Zhao, M.: Global-scale Attribution of Anthropogenic and
579 Natural Dust Sources and Their Emission Rates Based on MODIS Deep Blue Aerosol Products, Rev. Geophys., 50,
580 RG3005, doi: 3010.1029/2012RG000388, 2012.
581 Goodman, A. L., Bernard, E. T., and Grassian, V. H.: Spectroscopic Study of Nitric Acid and Water Adsorption on
582 Oxide Particles: Enhanced Nitric Acid Uptake Kinetics in the Presence of Adsorbed Water, J. Phys. Chem. A, 105,
583 6443-6457, 2001.
584 Gu, W. J., Li, Y. J., Zhu, J. X., Jia, X. H., Lin, Q. H., Zhang, G. H., Ding, X., Song, W., Bi, X. H., Wang, X. M., and
585 Tang, M. J.: Investigation of water adsorption and hygroscopicity of atmospherically relevant particles using
586 a commercial vapor sorption analyzer, Atmos. Meas. Tech., 10, 3821-3832, 2017.
587 Gustafsson, R. J., Orlov, A., Badger, C. L., Griffiths, P. T., Cox, R. A., and Lambert, R. M.: A comprehensive
588 evaluation of water uptake on atmospherically relevant mineral surfaces: DRIFT spectroscopy, thermogravimetric
589 analysis and aerosol growth measurements, Atmos. Chem. Phys., 5, 3415-3421, 2005.
590 Hall, P. L., and Astill, D. M.: Adsorption of water by homoionic exchange forms of Wyoming Montmorillonite
591 (SWy-1), Clays and Clay Minerals, 37, 355-363, 1989.
592 Hatch, C. D., Gierlus, K. M., Schuttlefield, J. D., and Grassian, V. H.: Water adsorption and cloud condensation
593 nuclei activity of calcite and calcite coated with model humic and fulvic acids, Atmos. Environ., 42, 5672-5684,
594 2008.
595 Hatch, C. D., Wiese, J. S., Crane, C. C., Harris, K. J., Kloss, H. G., and Baltrusaitis, J.: Water Adsorption on Clay
596 Minerals As a Function of Relative Humidity: Application of BET and Freundlich Adsorption Models, Langmuir,
597 28, 1790-1803, 2011.
598 Hatch, C. D., Greenaway, A. L., Christie, M. J., and Baltrusaitis, J.: Water adsorption constrained Frenkel–Halsey–
599 Hill adsorption activation theory: Montmorillonite and illite, Atmos. Environ., 87, 26-33, 2014.
600 Hatch, C. D., Tumminello, P. R., Cassingham, M. A., Greenaway, A. L., Meredith, R., and Christie, M. J.: Technical
601 note: Frenkel, Halsey and Hill analysis of water on clay minerals: toward closure between cloud condensation nuclei
602 activity and water adsorption, Atmos. Chem. Phys., 19, 13581-13589, 2019.
603 He, H., Wang, Y., Ma, Q., Ma, J., Chu, B., Ji, D., Tang, G., Liu, C., Zhang, H., and Hao, J.: Mineral Dust and NOx
604 Promote the Conversion of $SO_2$ to Sulfate in Heavy Pollution Days, Sci. Rep., 4, 4172, 2014.
605 Herich, H., Tritscher, T., Wiacek, A., Gysel, M., Weingartner, E., Lohmann, U., Baltensperger, U., and Cziczo, D.
606 J.: Water uptake of clay and desert dust aerosol particles at sub- and supersaturated water vapor conditions, Phys.
607 Chem. Chem. Phys., 11, 7804-7809, 2009.
608 Hiranuma, N., Augustin-Bauditz, S., Bingemer, H., Budke, C., Curtius, J., Danielczok, A., Diehl, K., Dreischmeier,
609 K., Ebert, M., Frank, F., Hoffmann, N., Kandler, K., Kiselev, A., Koop, T., Leisner, T., Möhler, O., Nillius, B.,
610 Peckhaus, A., Rose, D., Weinbruch, S., Wex, H., Boose, Y., DeMott, P. J., Hader, J. D., Hill, T. C. J., Kanji, Z. A.,
611 Kulkarni, G., Levin, E. J. T., McCluskey, C. S., Murakami, M., Murray, B. J., Niedermeier, D., Petters, M. D.,
612 O'Sullivan, D., Saito, A., Schill, G. P., Tajiri, T., Tolbert, M. A., Welti, A., Whale, T. F., Wright, T. P., and
613 Yamashita, K.: A comprehensive laboratory study on the immersion freezing behavior of illite NX particles: a
614 comparison of 17 ice nucleation measurement techniques, Atmos. Chem. Phys., 15, 2489-2518, 2015.

https://doi.org/10.5194/acp-2020-442
Preprint. Discussion started: 25 May 2020
© Author(s) 2020. CC BY 4.0 License.

Atmospheric Chemistry and Physics Discussions

615 Huang, J. P., Wang, T. H., Wang, W. C., Li, Z. Q., and Yan, H. R.: Climate effects of dust aerosols over East Asian
616 arid and semiarid regions, J. Geophys. Res.-Atmos., 119, 11398-11416, 2014.
617 Huneeus, N., Schulz, M., Balkanski, Y., Griesfeller, J., Prospero, J., Kinne, S., Bauer, S., Boucher, O., Chin, M.,
618 Dentener, F., Diehl, T., Easter, R., Fillmore, D., Ghan, S., Ginoux, P., Grini, A., Horowitz, L., Koch, D., Krol, M.
619 C., Landing, W., Liu, X., Mahowald, N., Miller, R., Morcrette, J. J., Myhre, G., Penner, J., Perlwitz, J., Stier, P.,
620 Takemura, T., and Zender, C. S.: Global dust model intercomparison in AeroCom phase I, Atmos. Chem. Phys., 11,
621 7781-7816, 2011.
622 Hung, H. M., Wang, K. C., and Chen, J. P.: Adsorption of nitrogen and water vapor by insoluble particles and the
623 implication on cloud condensation nuclei activity, J. Aerosol. Sci., 86, 24-31, 2015.
624 Ibrahim, S., Romanias, M. N., Alleman, L. Y., Zeineddine, M. N., Angeli, G. K., Trikalitis, P. N., and Thevenet, F.:
625 Water Interaction with Mineral Dust Aerosol: Particle Size and Hygroscopic Properties of Dust, ACS Earth and
626 Space Chem., 2, 376-386, 2018.
627 Jickells, T. D., An, Z. S., Andersen, K. K., Baker, A. R., Bergametti, G., Brooks, N., Cao, J. J., Boyd, P. W., Duce,
628 R. A., Hunter, K. A., Kawahata, H., Kubilay, N., laRoche, J., Liss, P. S., Mahowald, N., Prospero, J. M., Ridgwell,
629 A. J., Tegen, I., and Torres, R.: Global Iron Connections between Desert Dust, Ocean Biogeochemistry, and
630 Climate, Science, 308, 67-71, 2005.
631 Joshi, N., Romanias, M. N., Riffault, V., and Thevenet, F.: Investigating water adsorption onto natural mineral dust
632 particles: Linking DRIFTS experiments and BET theory, Aeolian Res., 27, 35-45, 2017.
633 Journet, E., Balkanski, Y., and Harrison, S. P.: A New Data Set of Soil Mineralogy for Dust-cycle Modeling, Atmos.
634 Chem. Phys., 14, 3801-3816, 2014.
635 Karydis, V. A., Tsimpidi, A. P., Bacer, S., Pozzer, A., Nenes, A., and Lelieveld, J.: Global impact of mineral dust on
636 cloud droplet number concentration, Atmos. Chem. Phys., 17, 5601-5621, 2017.
637 Ketteler, G., Yamamoto, S., Bluhm, H., Andersson, K., Starr, D. E., Ogletree, D. F., Ogasawara, H., Nilsson, A., and
638 Salmeron, M.: The Nature of Water Nucleation Sites on TiO2(110) Surfaces Revealed by Ambient Pressure X-ray
639 Photoelectron Spectroscopy, J. Phys. Chem. C, 111, 8278-8282, 2007.
640 Knippertz, P., and Stuut, J. B. W.: Mineral Dust: A Key Player in the Earth System, Springer, Dordrecht, 2014.
641 Koehler, K. A., Kreidenweis, S. M., DeMott, P. J., Petters, M. D., Prenni, A. J., and Carrico, C. M.: Hygroscopicity
642 and cloud droplet activation of mineral dust aerosol, Geophys. Res. Lett., 36, L08805, doi:
643 08810.01029/02009gl037348, 2009.
644 Kreidenweis, S. M., and Asa-Awuku, A.: 5.13 - Aerosol Hygroscopicity: Particle Water Content and Its Role in
645 Atmospheric Processes, in: Treatise on Geochemistry (Second Edition), edited by: Turekian, K. K., Elsevier,
646 Oxford, 331-361, 2014.
647 Kumar, P., Sokolik, I. N., and Nenes, A.: Parameterization of cloud droplet formation for global and regional
648 models: including adsorption activation from insoluble CCN, Atmos. Chem. Phys., 9, 2517-2532, 2009.
649 Kumar, P., Sokolik, I. N., and Nenes, A.: Cloud condensation nuclei activity and droplet activation kinetics of wet
650 processed regional dust samples and minerals, Atmos. Chem. Phys., 11, 8661-8676, 2011a.
651 Kumar, P., Sokolik, I. N., and Nenes, A.: Measurements of cloud condensation nuclei activity and droplet activation
652 kinetics of fresh unprocessed regional dust samples and minerals, Atmos. Chem. Phys., 11, 3527-3541, 2011b.
653 Laaksonen, A., Malila, J., Nenes, A., Hung, H. M., and Chen, J. P.: Surface fractal dimension, water adsorption
654 efficiency, and cloud nucleation activity of insoluble aerosol, Sci. Rep., 6, 25504, doi: 25510.21038/srep25504,
655 2016.
656 Lasne, J., Romanias, M. N., and Thevenet, F.: Ozone Uptake by Clay Dusts under Environmental Conditions, Acs
657 Earth and Space Chemistry, 2, 904-914, 2018.
658 Li, R., Jia, X. H., Wang, F., Ren, Y., Wang, X., Zhang, H. H., Li, G. H., Wang, X. M., and Tang, M. J.:
659 Heterogeneous reaction of NO2 with hematite, goethite and magnetite: Implications for nitrate formation and iron
660 solubility enhancement, Chemosphere, 242, 125273, 2020.
661 Li, W. J., Xu, L., Liu, X. H., Zhang, J. C., Lin, Y. T., Yao, X. H., Gao, H. W., Zhang, D. Z., Chen, J. M., Wang, W.
662 X., Harrison, R. M., Zhang, X. Y., Shao, L. Y., Fu, P. Q., Nenes, A., and Shi, Z. B.: Air pollution–aerosol
663 interactions produce more bioavailable iron for ocean ecosystems, Science Adv., 3, e1601749, 2017.
664 Ma, Q. X., He, H., and Liu, Y. C.: In Situ DRIFTS Study of Hygroscopic Behavior of Mineral Aerosol, J. Environ.
665 Sci., 22, 555-560, 2010a.
666 Ma, Q. X., Liu, Y. C., and He, H.: The Utilization of Physisorption Analyzer for Studying the Hygroscopic
667 Properties of Atmospheric Relevant Particles, J. Phys. Chem. A, 114, 4232-4237, 2010b.
668 Ma, Q. X., Liu, Y. C., Liu, C., and He, H.: Heterogeneous Reaction of Acetic Acid on MgO, α-$Al_2O_3$, and $CaCO_3$
669 and the Effect on the Hygroscopic Behavior of These Particles, Phys. Chem. Chem. Phys., 14, 8403-8409, 2012a.

https://doi.org/10.5194/acp-2020-442
Preprint. Discussion started: 25 May 2020
© Author(s) 2020. CC BY 4.0 License.

Atmospheric Chemistry and Physics Discussions


Ma, Q. X., Liu, Y. C., Liu, C., Ma, J. Z., and He, H.: A case study of Asian dust storm particles: Chemical composition, reactivity to SO2 and hygroscopic properties, J. Environ. Sci., 24, 62-71, 2012b.

Meskhidze, N., Volker, C., Al-Abadleh, H. A., Barbeau, K., Bressac, M., Buck, C., Bundy, R. M., Croot, P., Feng, Y., Ito, A., Johansen, A. M., Landing, W. M., Mao, J. Q., Myriokefalitakis, S., Ohnemus, D., Pasquier, B., and Ye, Y.: Perspective on identifying and characterizing the processes controlling iron speciation and residence time at the atmosphere-ocean interface, Mar. Chem., 217, 103704, doi: 103710.101016/j.marchem.102019.103704, 2019.

Mitroo, D., Gill, T. E., Haas, S., Pratt, K. A., and Gaston, C. J.: ClNO2 production from N2O5 uptake on saline playa dusts: New insights into potential inland sources of ClNO2, Environ. Sci. Technol., 13, 7442-7452, 2019.

Navea, J. G., Chen, H. H., Huang, M., Carmichael, G. R., and Grassian, V. H.: A comparative evaluation of water uptake on several mineral dust sources, Environ. Chem., 7, 162-170, 2010.

Nickovic, S., Vukovic, A., Vujadinovic, M., Djurdjevic, V., and Pejanovic, G.: Technical Note: High-resolution mineralogical database of dust-productive soils for atmospheric dust modeling, Atmos. Chem. Phys., 12, 845-855, 2012.

Okin, G. S., Baker, A. R., Tegen, I., Mahowald, N. M., Dentener, F. J., Duce, R. A., Galloway, J. N., Hunter, K., Kanakidou, M., Kubilay, N., Prospero, J. M., Sarin, M., Surapipith, V., Uematsu, M., and Zhu, T.: Impacts of atmospheric nutrient deposition on marine productivity: Roles of nitrogen, phosphorus, and iron, Glob. Biogeochem. Cycle, 25, GB2022, doi: 2010.1029/2010GB003858, 2011.

Rubasinghege, G., and Grassian, V. H.: Role(s) of Adsorbed Water in the Surface Chemistry of Environmental Interfaces, Chem. Commun., 49, 3071-3094, 2013.

Scanza, R. A., Mahowald, N., Ghan, S., Zender, C. S., Kok, J. F., Liu, X., Zhang, Y., and Albani, S.: Modeling Dust as Component Minerals in the Community Atmosphere Model: Development of Framework and Impact on Radiative Forcing, Atmos. Chem. Phys., 15, 537-561, 2015.

Schulz, M., Prospero, J. M., Baker, A. R., Dentener, F., Ickes, L., Liss, P. S., Mahowald, N. M., Nickovic, S., García-Pando, C. P., Rodríguez, S., Sarin, M., Tegen, I., and Duce, R. A.: Atmospheric Transport and Deposition of Mineral Dust to the Ocean: Implications for Research Needs, Environ. Sci. Technol., 46, 10390-10404, 2012.

Schuttlefield, J., Al-Hosney, H., Zachariah, A., and Grassian, V. H.: Attenuated Total Reflection Fourier Transform Infrared Spectroscopy to Investigate Water Uptake and Phase Transitions in Atmospherically Relevant Particles, Appl. Spectrosc., 61, 283-292, 2007a.

Schuttlefield, J. D., Cox, D., and Grassian, V. H.: An investigation of water uptake on clays minerals using ATR-FTIR spectroscopy coupled with quartz crystal microbalance measurements, J. Geophys. Res.-Atmos., 112, D21303, doi: 21310.21029/22007JD008973, 2007b.

Schuttlefield, J. D.: Laboratory Studies of Reactions of Atmospheric Gases with Components of Mineral Dust Aerosol and Research in Chemical Education, Ph. D., University of Iowa, 2008.

Sorjamaa, R., and Laaksonen, A.: The effect of $H_2O$ adsorption on cloud drop activation of insoluble particles: a theoretical framework, Atmos. Chem. Phys., 7, 6175-6180, 2007.

Sullivan, R. C., Minambres, L., DeMott, P. J., Prenni, A. J., Carrico, C. M., Levin, E. J. T., and Kreidenweis, S. M.: Chemical processing does not always impair heterogeneous ice nucleation of mineral dust particles, Geophys. Res. Lett., 37, L24805, doi: 24810.21029/22010GL045540, 2010a.

Sullivan, R. C., Moore, M. J. K., Petters, M. D., Kreidenweis, S. M., Qafoku, O., Laskin, A., Roberts, G. C., and Prather, K. A.: Impact of Particle Generation Method on the Apparent Hygroscopicity of Insoluble Mineral Particles, Aerosol Sci. Technol., 44, 830-846, 2010b.

Tagliabue, A., Bowie, A. R., Boyd, P. W., Buck, K. N., Johnson, K. S., and Saito, M. A.: The integral role of iron in ocean biogeochemistry, Nature, 543, 51-59, 2017.

Tang, M. J., Thieser, J., Schuster, G., and Crowley, J. N.: Kinetics and Mechanism of the Heterogeneous Reaction of $N_2O_5$ with Mineral Dust Particles, Phys. Chem. Chem. Phys., 14, 8551-8561, 2012.

Tang, M. J., Schuster, G., and Crowley, J. N.: Heterogeneous Reaction of $N_2O_5$ with Illite and Arizona Test Dust Particles, Atmos. Chem. Phys., 14, 245-254, 2014.

Tang, M. J., Cziczo, D. J., and Grassian, V. H.: Interactions of Water with Mineral Dust Aerosol: Water Adsorption, Hygroscopicity, Cloud Condensation and Ice Nucleation, Chem. Rev., 116, 4205–4259, 2016.

Tang, M. J., Huang, X., Lu, K. D., Ge, M. F., Li, Y. J., Cheng, P., Zhu, T., Ding, A. J., Zhang, Y. H., Gligorovski, S., Song, W., Ding, X., Bi, X. H., and Wang, X. M.: Heterogeneous reactions of mineral dust aerosol: implications for tropospheric oxidation capacity, Atmos. Chem. Phys., 17, 11727-11777, 2017.

Tang, M. J., Chan, C. K., Li, Y. J., Su, H., Ma, Q. X., Wu, Z. J., Zhang, G. H., Wang, Z., Ge, M. F., Hu, M., He, H., and Wang, X. M.: A review of experimental techniques for aerosol hygroscopicity studies, Atmos. Chem. Phys., 19, 12631-12686, 2019a.

https://doi.org/10.5194/acp-2020-442
Preprint. Discussion started: 25 May 2020
© Author(s) 2020. CC BY 4.0 License.

Atmospheric Chemistry and Physics Discussions

Tang, M. J., Gu, W. J., Ma, Q. X., Li, Y. J., Zhong, C., Li, S., Yin, X., Huang, R. J., He, H., and Wang, X. M.: Water adsorption and hygroscopic growth of six anemophilous pollen species: the effect of temperature, Atmos. Chem. Phys., 19, 2247-2258, 2019b.

Tang, M. J., Zhang, H. H., Gu, W. J., Gao, J., Jian, X., Shi, G. L., Zhu, B. Q., Xie, L. H., Guo, L. Y., Gao, X. Y., Wang, Z., Zhang, G. H., and Wang, X. M.: Hygroscopic Properties of Saline Mineral Dust From Different Regions in China: Geographical Variations, Compositional Dependence, and Atmospheric Implications, J. Geophys. Res.-Atmos, 124, 10844-10857, 2019c.

Textor, C., Schulz, M., Guibert, S., Kinne, S., Balkanski, Y., Bauer, S., Berntsen, T., Berglen, T., Boucher, O., Chin, M., Dentener, F., Diehl, T., Easter, R., Feichter, H., Fillmore, D., Ghan, S., Ginoux, P., Gong, S., Grini, A., Hendricks, J., Horowitz, L., Huang, P., Isaksen, I., Iversen, I., Kloster, S., Koch, D., Kirkevåg, A., Kristjansson, J. E., Krol, M., Lauer, A., Lamarque, J. F., Liu, X., Montanaro, V., Myhre, G., Penner, J., Pitari, G., Reddy, S., Seland, Ø., Stier, P., Takemura, T., and Tie, X.: Analysis and Quantification of the Diversities of Aerosol Life Cycles within AeroCom, Atmos. Chem. Phys., 6, 1777-1813, 2006.

Usher, C. R., Michel, A. E., and Grassian, V. H.: Reactions on Mineral Dust, Chem. Rev., 103, 4883-4939, 2003.

Vlasenko, A., Sjogren, S., Weingartner, E., Gaggeler, H. W., and Ammann, M.: Generation of submicron Arizona test dust aerosol: Chemical and hygroscopic properties, Aerosol Sci. Technol., 39, 452-460, 2005.

Vlasenko, A., Huthwelker, T., Gaggeler, H. W., and Ammann, M.: Kinetics of the heterogeneous reaction of nitric acid with mineral dust particles: an aerosol flow tube study, Phys. Chem. Chem. Phys., 11, 7921-7930, 2009.

Wang, T., Liu, Y., Deng, Y., Fu, H., Zhang, L., and Chen, J.: Adsorption of SO2 on mineral dust particles influenced by atmospheric moisture, Atmos. Environ., 191, 153-161, 2018.

Xu, W. Z., Johnston, C. T., Parker, P., and Agnew, S. F.: Infrared study of water sorption on Na-, Li-, Ca-, and Mg-exchanged (SWy-1 and SAz-1) montmorillonite, Clays Clay Miner., 48, 120-131, 2000.

Yeşilbaş, M., and Boily, J.-F.: Particle Size Controls on Water Adsorption and Condensation Regimes at Mineral Surfaces, Sci. Rep., 6, 32136, doi: 32110.31038/srep32136, 2016.

Yu, Z., and Jang, M.: Simulation of heterogeneous photooxidation of SO2 and NOx in the presence of Gobi Desert dust particles under ambient sunlight, Atmos. Chem. Phys., 18, 14609-14622, 2018.

Yu, Z., and Jang, M.: Atmospheric Processes of Aromatic Hydrocarbons in the Presence of Mineral Dust Particles in an Urban Environment, ACS Earth and Space Chemistry, 3, 2404-2414, 2019.

Zent, A. P., Howard, D. J., and Quinn, R. C.: H2O adsorption on smectites: Application to the diurnal variation of H2O in the Martian atmosphere, J. Geophys. Res.-Planets, 106, 14667-14674, 2001.